

The Bingham Canyon Porphyry Cu-Mo-Au Deposit. II. Vein Geometry and Ore Shell Formation by Pressure-Driven Rock Extension

GILLIAN GRUEN,^{1,†} CHRISTOPH A. HEINRICH,² AND KIM SCHROEDER³

¹ Department of Earth Sciences, ETH Zurich, 8092 Zurich, Switzerland

² Department of Earth Sciences, ETH Zurich, 8092 Zurich, Switzerland, and
Faculty of Mathematics and Natural Sciences, University of Zurich

³ Kennecott Utah Copper, Rio Tinto, Magna, Utah 84044

Abstract

Copper, gold, and molybdenum in the Bingham Canyon deposit (Utah, United States) show a systematic distribution in grade and metal ratios. Most Cu-Au mineralization follows, both spatially and temporally, the emplacement of the quartz monzonite porphyry (QMP), a southwest-northeast-elongated thick dike intruding along the contact between the premineralization equigranular monzonite stock and surrounding sedimentary rocks. Copper ore grades define the shape of an inverted cup, which is centered on the QMP but has a much broader, near-circular footprint. Several deep root zones surround a barren core occupied by the same lithologic units and intense potassic alteration but insignificant metal tenor. Throughout the deposit, gold to copper ratio is systematically zoned. The distribution of molybdenum resembles that of copper and partly overlaps with it, but the molybdenum ore shell is generally displaced inward and downward from the copper ore shell.

Systematic measurement of the abundance and orientation of three major vein types obtained at the pit surface were complemented with unoriented vein density data from drill core logging. Quartz stockwork veins, the earliest and most abundant of the mapped vein types, are related to potassic alteration and major Cu-Au mineralization. Their greatest vein density follows the intrusion of the QMP but extends far beyond, into sedimentary rocks and especially into adjacent parts of the pre-ore equigranular monzonite. Their orientation is predominantly steep, with a variable strike. Quartz-molybdenite veins postdate all intrusions and are less abundant than quartz stockwork veins. They show variable orientation of strikes and a weaker tendency to steep dips. Quartz-pyrite veins with sericitic alteration halos crosscut all intrusions and earlier veins. They are rare within the central high-grade part of the deposit and predominantly occur near and outside the northeastern and southwestern ends of the QMP. They have a strongly preferred orientation parallel to the porphyry dikes, with steep dips and strike directions fanning out radially from the center of the deposit.

Repeated cycles of dike intrusions with distinct southwest-northeast orientation, followed by steep stockwork veins with variable strikes distributed over the broad ore shell and a final return to oriented postore veins are interpreted to result from alternation between two stress regimes. A regional, probably weakly transtensional regime controls the emplacement of dikes and postore veins. Ore vein formation and mineralization is controlled by active rock extension (increase in differential stress) in the roof area above a broad region of high fluid pressure in a subjacent magma chamber, rather than by local hydrofracturing caused by fluid exsolution from the porphyries (decrease in effective rock pressure and positive volume change upon magma crystallization). Shallow vein mineralization well above the lithostatic-to-hydrostatic transition is consistent with low (hydrostatic or even vapor-static) pressures of ore deposition indicated by a companion study of fluid inclusions. The process of pressure-driven roof extension favors the accumulation of metals in high-grade ore shells, compared to temperature-driven concepts according to which the porphyry mineralization is spread out vertically by following downward-retracting isotherms in a cooling magmatic-hydrothermal system.

Introduction

PORPHYRY-STYLE and epithermal Cu-Mo-Au-Ag ore deposits are controlled by tectonic processes operating at variable scales, from the convergence of lithospheric plates to the formation of individual ore veins (Sawkins, 1990; Sillitoe, 2010). Ore-forming hydrothermal processes operate in the upper 10 km of crust, at the interface between the shallow ground-water environment and a hydrous magma regime extending to mantle depths (Sillitoe, 1972; Beane and Titley, 1981; Richards, 2003; Seedorff et al., 2005; Williams-Jones and Heinrich, 2005).

The deep magmatic regime acts as a source of heat, magmatic volatiles, and ore-forming components. Exposed lower- to mid-crustal magma chambers in arc settings are horizontally layered and have sill-like shapes (e.g., Jagoutz et al., 2007). Horizontal

compression of the lithosphere facilitates magma storage and high-pressure differentiation toward volatile-rich magmas (Tosdal and Richards, 2001; Annen and Sparks, 2002; Richards, 2003; Rohrlach et al., 2003; Rohrlach and Loucks, 2005). A compressive regime in the upper crust prevents magma chambers from erupting through volcanoes. Instead, it favors focused loss of volatiles through hydraulically fractured porphyry stocks in the roof of the intrusions (Burnham, 1979; Dilles, 1987; Richards, 2003; Rohrlach and Loucks, 2005; Sillitoe and Perello, 2005). Fluids exsolve from magma chambers under near-lithostatic pressure (Burnham and Ohmoto, 1980; Fournier, 1999), as required to open flat veins in deep magmatic-hydrothermal deposits like Panasqueira (Kelly and Rye, 1979).

Acronyms Used in this Paper

LP = latite porphyry

QLP = quartz latite porphyry

QMP = quartz monzonite porphyry

[†] Corresponding author: e-mail, gruen@erdw.ethz.ch

By contrast, structures in the depositional regime of porphyry-style and epithermal ore deposits are typically steep, with subvertical intrusive contacts of porphyry stocks and dikes (e.g., Seedorff et al., 2005; Sillitoe, 2010), radial or concentric veins in porphyry copper deposits (Heidrick and Titley, 1982), and large subvertical veins in epithermal ore deposits and active geothermal systems (Berger and Bethke, 1985; Simmons et al., 2005). Porphyries with mineralized vein stockworks are commonly emplaced at sites where transtensional deformation produces vertical extensional volumes such as fault jogs channeling the ascent of magma and fluids (Titley, 1982; Fournier, 1999; Tosdal and Richards, 2001; Cannell et al., 2005; Sillitoe and Perello, 2005).

The transition from predominantly flat to predominantly steep structures reflects a vertical transition in the state of differential rock stress and fluid pressure (Fournier, 1999; Cox, in press). Several structural studies of porphyry vein networks have documented and discussed the nature of this transition (Beane and Titley, 1981; Heidrick and Titley, 1982; Titley, 2001). Recent geodetic data provide additional insights into the mechanisms of magma emplacement and fluid expulsion into upper-crustal hydrothermal systems, emphasizing vertical uplift and radial extension (Bonafede, 1991; Todesco et al., 2004; Hurwitz et al., 2007; Bodnar et al., 2007; Dzurisin et al., 2009; Hutnak et al., 2009; Lima et al., 2009).

Bingham Canyon near Salt Lake City (Utah, United States) is a giant porphyry Cu-Mo-Au deposit exhibiting clear geometric relationships between intrusions, different vein generations, and a regular distribution of Cu, Au, and Mo in a zoned ore shell, which is exposed over 2.3 km of vertical extent thanks to 100 years of open-pit mining and deep diamond drilling. Building on the detailed geologic relationships shown in the preceding article (Redmond and Einaudi, 2010), this paper presents the three-dimensional distribution of ore metals in relationship to fracture density and orientations of the evolving vein network. Our analysis aims at understanding the physical evolution of vein opening and focused fluid flow, in an attempt to relate the emplacement of intrusions and veins to the interplay between far-field crustal stress of the region and the more localized stress and fluid pressure distribution caused by the underlying magmatic intrusion. These observations will be combined with a fluid inclusion study in the third companion paper, to explain the origin of the zoned Bingham ore shell as the product of an upward-expanding vapor plume above the lithostatic-to-hydrostatic transition (companion paper by Landtwing et al., 2010).

Tectonic Evolution, Deposit-Scale Geology, and Structures

The Bingham Canyon mining district ($\sim 112^{\circ}09'W/40^{\circ}30'N$) near Salt Lake City, Utah, is located at the eastern edge of the Basin and Range province, far inland from the former subduction zone during the Eocene (Fig. 1A). The magmatic-hydrothermal complex is located near the southern cratonic margin of the Wyoming province (Karlstrom et al., 2005) and extends along the east-west-oriented Uinta Axis, a basement uplift that probably coincides with a former intracontinental rift basin filled with Precambrian sedimentary rocks (Sears et al., 1982). The giant porphyry Cu-Mo-Au orebody, surrounded

by a district of smaller Cu-Au skarns and polymetallic vein and replacement deposits, is controlled by structural elements dating back to the Precambrian (Sears et al., 1982; Bryant, 1988; Bryant and Nichols, 1988; Presnell, 1998).

Precambrian to Mesozoic tectonism

Sedimentary rocks in the mine area consist of quartzite and lesser limestone, calcareous siltstone, and sandstone of the Pennsylvanian Oquirrh Group (Tooker et al., 1970; Swensen, 1975). Carbonate rocks of the Bingham Mine Formation host Cu-Au skarns and a halo of Pb-Zn-Ag fissure and replacement deposits such as the Lark mine east of the Bingham Canyon intrusions (Fig. 1B). About 8 km north of the Bingham Canyon mine, beyond the Pb-Zn halo but still within the outer Au-As limit, dolomitic and calcareous units host the Carlin-type gold deposits at Barneys Canyon and Melco (Cunningham et al., 2004; Fig. 1B). Prior to Eocene magmatism, the mid Jurassic Elko orogeny and the Late Cretaceous Sevier orogeny have affected the region (Presnell, 1992; Babcock et al., 1995; Presnell and Parry, 1995). These compressional periods formed two major fold sets including the Copperton anticline (Fig. 1B) and the northwest-trending, overturned Apex and Rood folds (Fig. 2). These folds are separated by the southwest-dipping Midas thrust, which resulted from eastward compression during the Sevier orogeny (Fig. 1B).

Eocene magmatism

Igneous activity along the Uinta axis (Fig. 1A) started at a time when tectonic activity in western North America was generally shifting eastward due to low-angle subduction (English and Johnston, 2004). Minor Eocene extension was followed by an intense period of Eocene intrusive and volcanic activity (Presnell, 1992, 1998), forming the west-trending Wasatch igneous belt extending from the Park City mineral district (John, 1998) through the more deeply exposed Alta stock (Cook and Bowman, 2000), across the later Wasatch fault into the Oquirrh Mountains (Fig. 1A). A positive aeromagnetic anomaly indicates a large west-trending batholith underlying the entire Uinta axis, including the Bingham Canyon magmatic complex (Waite et al., 1998).

The Bingham Canyon magmatic complex comprises at least five phases of petrographically distinct intrusions (Redmond and Einaudi, 2010; Fig. 2). The equigranular monzonite pre-dates all hydrothermal mineralization and include the large Last Chance stock (unaltered and occurring immediately south of the Bingham Canyon mine) and the Bingham Stock (occupying most of the open pit; Babcock et al., 1995). Despite its geometric complexity, the equigranular monzonite is approximately equidimensional in outcrop area and has steep walls, based on drilling and unpublished geophysical data processing (I. Steinberger, pers. commun.). The quartz monzonite porphyry (QMP) forms a northeast-striking, approximately 60° northwest-dipping, up to 500-m-thick dike-like body that intruded along the northwestern contact between the Bingham stock and sedimentary country rocks (Redmond and Einaudi, 2010, fig. 1). This porphyry is spatially and temporally related to most of the quartz stockwork veins, potassic alteration, and Cu-Au mineralization (John, 1978; Lanier et al., 1978; Warnaars et al., 1978; Redmond et al., 2002, 2004). Early studies (e.g., Boutwell et al., 1905) indicate that

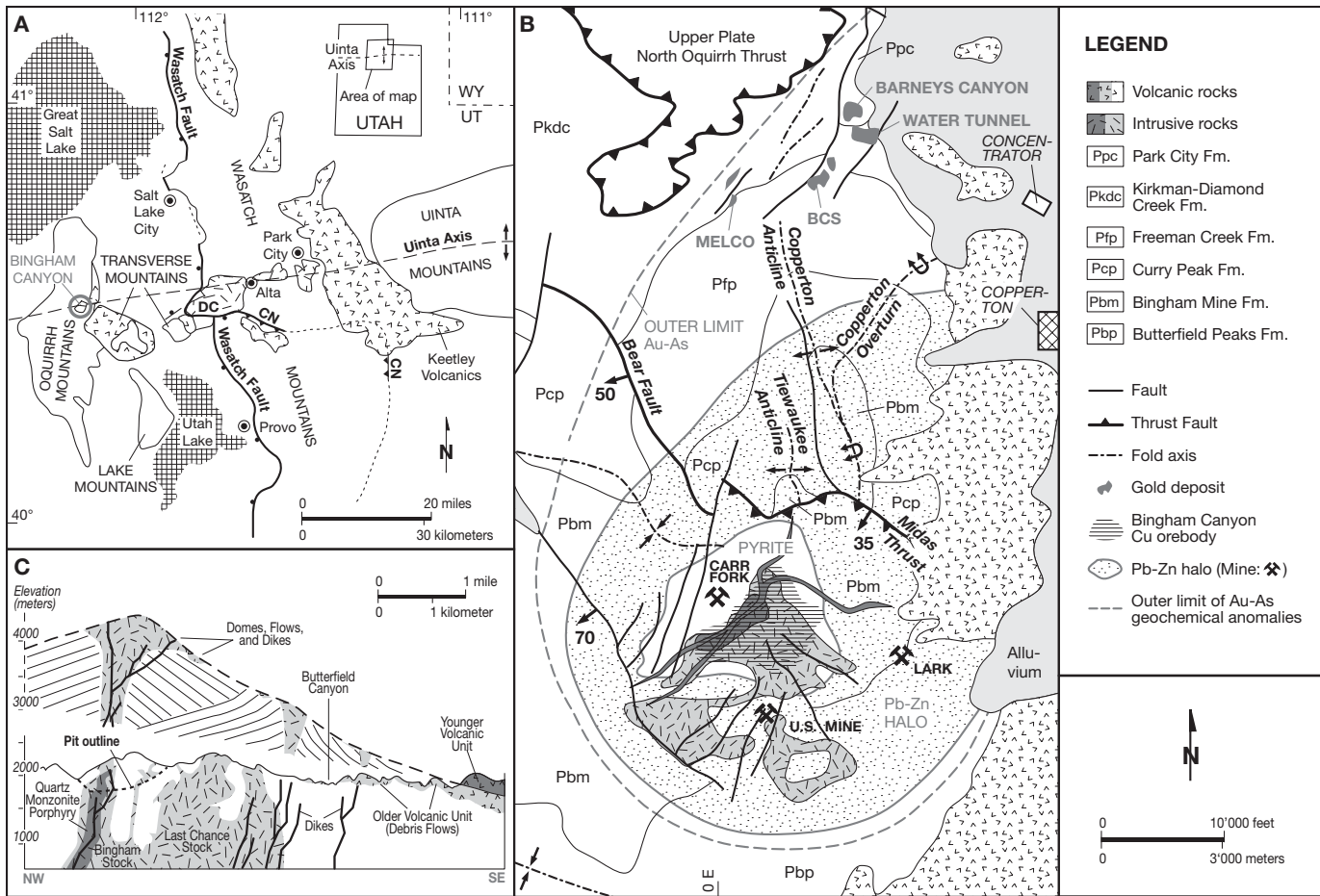


FIG. 1. Overview on the Bingham Canyon porphyry copper deposit. A. Index map of the central Wasatch Mountains and surrounding region in north-central Utah, showing the location of the Bingham Canyon mine, major folds, faults, and the distribution of Tertiary igneous rocks (modified from John, 1989, 1998); CN = Charleston-Nebo thrust, DC = Deer Creek fault. B. Geologic map of the Bingham district, showing ore deposits, metal zonation, and some major lithologic units and structures (modified from Babcock et al., 1995). C. Northwest-southeast-oriented cross section, showing the hypothetical volcanic edifice above the Bingham Canyon deposit (modified from Deino and Keith, 1998; Waite et al., 1998).

equigranular monzonite and QMP both cropped out at the premine surface, but there are no data to indicate whether the QMP extended to the paleosurface or closed just above the known Cu-Au orebody (K. Krahulec, pers. commun., 2006). Successively thinner dikes of latite porphyry (LP, up to 30 m thick), quartz latite porphyry (QLP) and minor dike types (Redmond and Einaudi, 2010) generally have steeply dipping (60° – 75°) contacts. They strike northeast through the center of the Bingham stock with a lateral extent over 8 km.

Some of the magmas vented to the surface, forming a composite volcano which is partly preserved on the eastern flank of the Oquirrh Mountains (Waite et al., 1998; Maughan et al., 2002; Fig. 1A). Latite lavas and volcanoclastic rocks here dip eastward under Late Tertiary and Quaternary cover of the Salt Lake basin. The volcanic sequence is at least 1 km thick and dominantly composed of porphyritic flow-layered andesite and dacite lavas, minor ash-flow tuffs and mud-flow breccias (Waite et al., 1998). Structural reconstructions indicate that the pre-mine surface of Bingham Canyon may have been overlain by ~2 km of volcanic and intrusive rocks (Fig. 1C, redrawn from Waite et al., 1998).

Faulting and folding

A set of north-northeast- to northeast-striking faults and fractures is developed throughout the Bingham Canyon district (Fig. 1B). These structures crosscut the equigranular monzonite and appear to have controlled the emplacement of the northeast-striking QMP and similarly striking later porphyry dikes (Atkinson and Einaudi, 1978; Presnell, 1998). They are also important controls for later Pb-Zn mineralization, including the historic Lark (eastern), U.S. Mine (southern), and Carr Fork (western) mining areas located within about 2.5 km from the QMP (Fig. 1B). Northwest-trending faults including the Copper Center fault and the Giant Chief fault seem to control jogs in the Latite Porphyry in the region of high-grade Cu-Au mineralization in the QMP (Fig. 2). The Bingham syncline is a northwest-striking broad open fold and is thought to be the result of folding caused by the intrusions (J. Grocott and A. Kloppenborg, pers. commun.). Other northwest-striking normal faults postdate mineralization and, along with reactivation on some northeast structures, reflect the onset of Miocene to recent Basin and Range extension (Presnell,

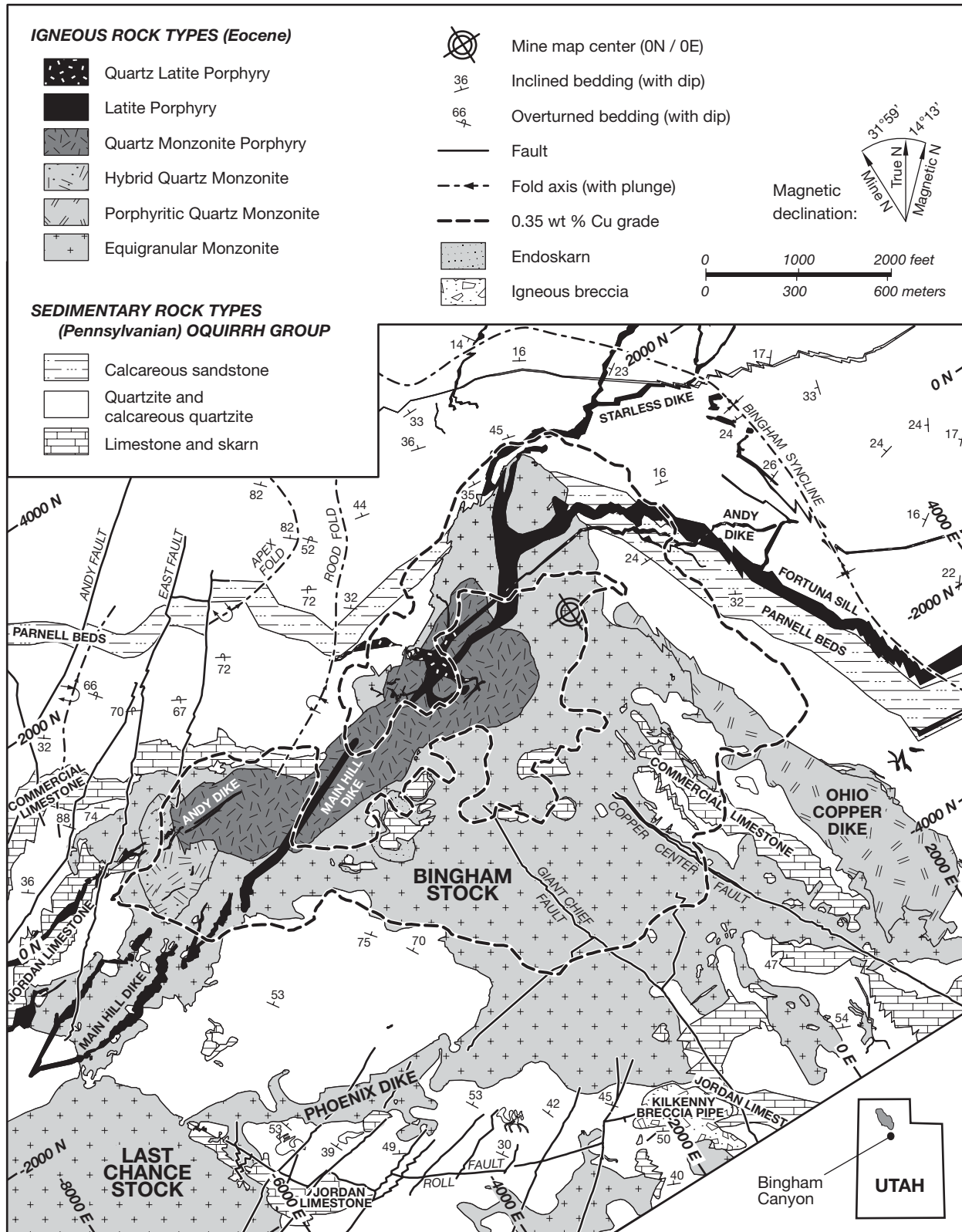


FIG. 2. Geologic map of the Bingham Canyon mine including lithologic units, major structures, and the area of >0.35 wt percent Cu grade outline as a contour to the pit surface (data from KUC, mapping of 2006 updated locally). Mine grid (ft) indicated with ticks.

1992, 1998). The modern Basin and Range topography is related to extension along broadly north-trending faults (Zoback, 1983; Constenius, 1996). The Wasatch fault is the easternmost bounding fault of the Basin and Range. It started moving at 18 to 17 Ma (Parry et al., 1988), opening the Salt Lake Valley by downfaulting the Oquirrh Mountains block with a 15° to 30° eastside down rotation (Smith, 1961; John, 1989; Melker and Geissman, 1998). This preserved the sub-volcanic ore deposits, while erosion of the upfaulted Wasatch Mountains exposed deep Eocene plutons that had been emplaced into Precambrian and Paleozoic rocks along the Uinta axis (Fig. 1).

Veins, Alteration, and Metal Zonation

Successive porphyry intrusions produced multiple generations of quartz veins associated with characteristic ore mineralization and wall-rock alteration. Zoned ore metal distribution closely relates to the type and intensity of veins and hydrothermal alteration of igneous rocks (Rose, 1970; Atkinson and Einaudi, 1978; John, 1978; Babcock et al., 1995; Phillips et al., 1998; Redmond et al., 2001; Redmond, 2002; Redmond and Einaudi, 2010). Continued updating of geology and ore-grade distribution by Rio Tinto's division Kennecott Utah Copper formed the basis of the construction of Figure 3. Despite a locally complex distribution of ore grades and alteration intensity, controlled by host lithologic units and fault structures (Redmond and Einaudi, 2010), the Bingham Canyon orebody shows an overall simple and systematic ore metal zonation, centered on the southeastern contact of the QMP (Fig. 2).

Quartz stockwork veins, potassic alteration, and Cu-Au distribution

Following several stages of volumetrically minor vein types (Redmond and Einaudi, 2010), several pulses of quartz stockwork veining, potassic alteration, and Cu-Au mineralization determined the large-scale distribution of copper and gold in the Bingham Canyon orebody.

Copper distribution: The distribution of copper best defines the overall shape of the Bingham Canyon orebody, as depicted by grade-envelope surfaces shown in Figure 3. The rock volume containing >0.35 wt percent Cu has the shape of a thick-walled inverted cup, as shown in the three-dimensional projection in Figure 3A (red body). The shape has also been compared to a molar tooth, to emphasize the thick crown and the irregular base of the peripheral zones of the Cu orebody, which has several deep roots extending below and beyond the margins of the already exploited orebody. Three peripheral root zones constitute the most important remaining Cu reserve of the mine. They are best developed outside the two ends of the thick QMP dike (the two dark red roots in the foreground of Fig. 3A) and below the southeastern periphery of the orebody in the equigranular monzonite (the fainter red lobe in background of Fig. 3A, located approximately beneath the outer 0.35 wt percent Cu contour shown in Fig. 2). Lower grade regions in the ring of deep peripheral ore zones tend to be in areas where quartzites predominate over the apparently more reactive equigranular monzonite. Although dikes of LP and later intrusions have successively lower Cu grades with locally sharp gradients at

intrusion contacts, the large-scale Cu distribution in the latite dikes follows the same pattern, with relatively highest grades in the region where they intrude the QMP and the immediately adjacent equigranular monzonite.

Gold distribution: Gold distribution shows a distinctly different shape than that of copper, giving rise to a systematic, deposit-scale zonation of the Au/Cu metal ratio (ppm Au per wt % Cu; Redmond et al., 2004). In the central zone of highest Cu grades in and surrounding the QMP, high Au grade correlates very closely with high Cu grade and both concentrations decrease parallel with each other in successive intrusion stages of latite dikes. On the scale of the entire deposit however (Fig. 3B, D), Au is concentrated in the region immediately in and around the QMP. Au and Cu concentrations show sharp and closely coinciding gradients at the base of this central Au-Cu orebody, irrespective of steeply dipping dike contacts. The central high-grade Au-Cu orebody contains an average of 0.8 wt percent Cu and 0.6 ppm Au. This results in a bulk Au/Cu ratio of 0.000075, which is significantly higher than the bulk Au/Cu ratio of the entire deposit (0.000042). High Au concentrations correlate systematically with the presence of bornite and digenite as the dominant Cu minerals. Towards the periphery, Au decreases more rapidly than Cu, i.e., the Au/Cu ratio decreases outward in a systematic manner. The peripheral deep roots of the orebody are Cu rich (>0.35 wt % over large volumes), but contain only 0.09 ppm Au in average, i.e. the Au/Cu ratio in the deep peripheral ore zones is lower than 0.000026. Consistently, Cu in the peripheral zones is predominantly present as chalcopyrite, whereas bornite or digenite are clearly subordinate.

Quartz stockwork veins (Fig. 4A): Quartz stockwork veins are closely related to Cu and Au grade and represent the channelways for fluids causing alteration of former mafic igneous minerals to biotite and of plagioclase to potassium feldspar in areas of most intense veining and potassic alteration. They include barren quartz veins and thin quartz sulfide veins, comparable to "A veins" and part of the "B veins" defined by Gustafson and Hunt (1975). Many samples show multiple generations of successively opened and quartz-filled fractures of changing and apparently random orientation (Fig. 4B), but some generations are represented by sheeted arrays of multiple parallel veins (Redmond and Einaudi, 2010). Quartz stockwork veins are typically 2 to 10 mm wide and can be followed for tens of centimeters, but wider and more extensive veins occur sporadically. At any one site, the earliest veins tend to be shorter, more diffuse, and with irregular walls indicating minor plastic deformation, whereas later veins are increasingly straight with granular to columnar quartz infill. Straight parallel-walled veins may have a centerline between quartz crystals grown perpendicularly from the vein walls, but the veins are generally completely filled. Lateral offsets of earlier veins by later ones indicate a component of shear displacement during vein opening (Fig. 4A). Evidence for shearing during quartz infill (e.g., sigmoidal quartz growth) is conspicuously absent. However, microbrecciation on the grain boundaries of earlier formed quartz crystals is ubiquitous (as seen by SEM-CL imaging; Redmond et al., 2004; Landtwing et al., 2005). Brecciation was associated with the precipitation of composite bornite-digenite grains, chalcopyrite and gold in secondary pore space formed by quartz

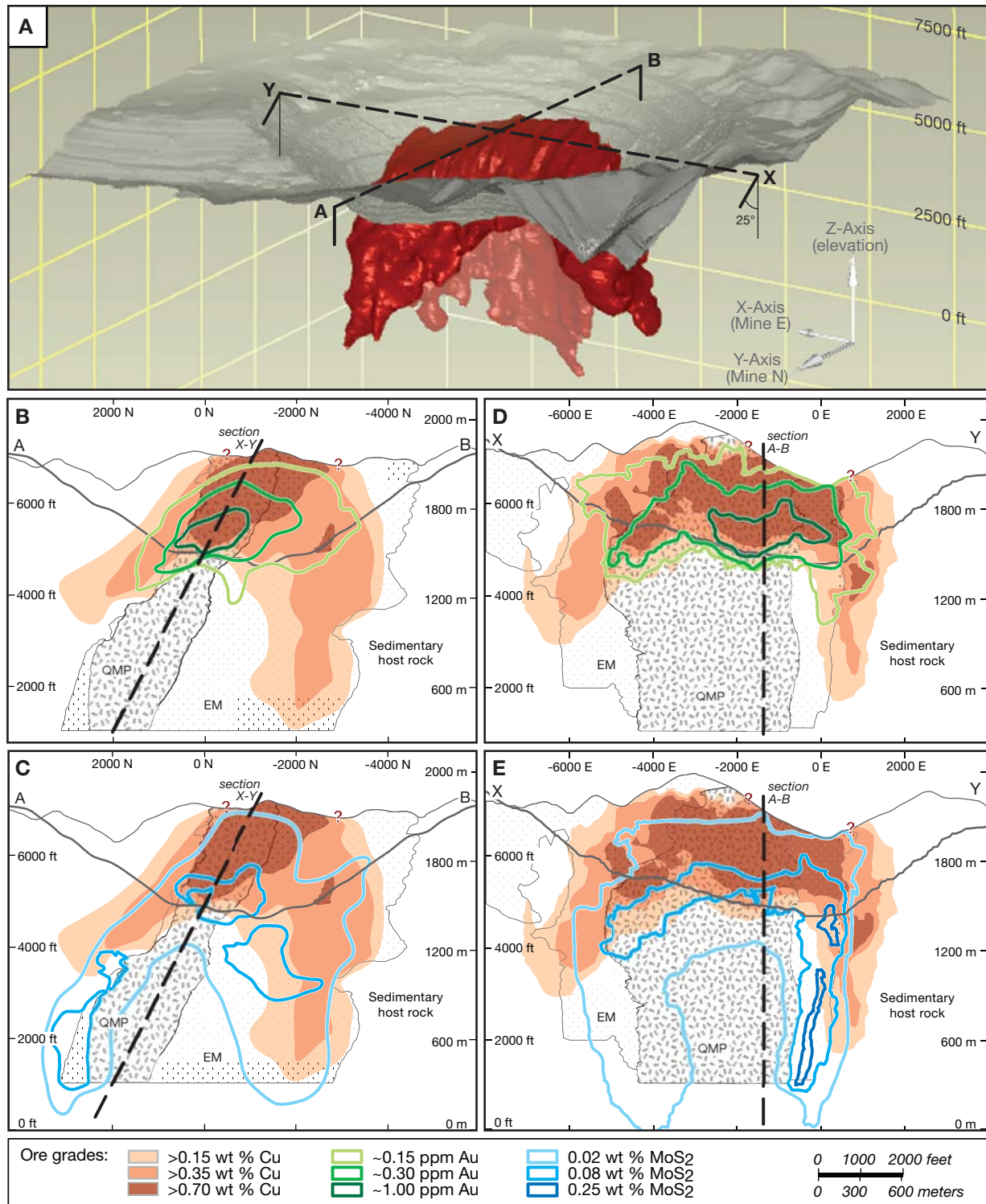


FIG. 3. Mine-scale distribution of Cu, Au, and Mo in the Bingham Canyon deposit, based on three-dimensional modeling data from KUC. Grid in mine coordinates (ft), orientations in text referred to True North, elevation above sea level. A. Three-dimensional view on the Bingham Canyon deposit, looking southeast. Shown are the 2006 topography (gray surface) and the envelope surface of >0.35 wt percent Cu (red body; already mined out above the open-pit surface). Orientations of cross sections are indicated; see Figure 7 for traces at surface map. B. and C. Vertical northwest-southeast cross section (A-B; azimuth relative to True North: 148°, dip: 90°, showing Cu grades (decreasing shades of brown) together with contours of Au (yellow to green in B) and MoS₂ (blue in C) concentrations, respectively. Traces of cross section X-Y are indicated. D. and E. Inclined southwest-northeast cross section following the QMP (X-Y; azimuth relative to True North: 58°, dip: 65° toward NW), showing the Cu, Au (D), and MoS₂ (E) distribution in the same colors as in B and C, respectively. Traces of cross section A-B are indicated.

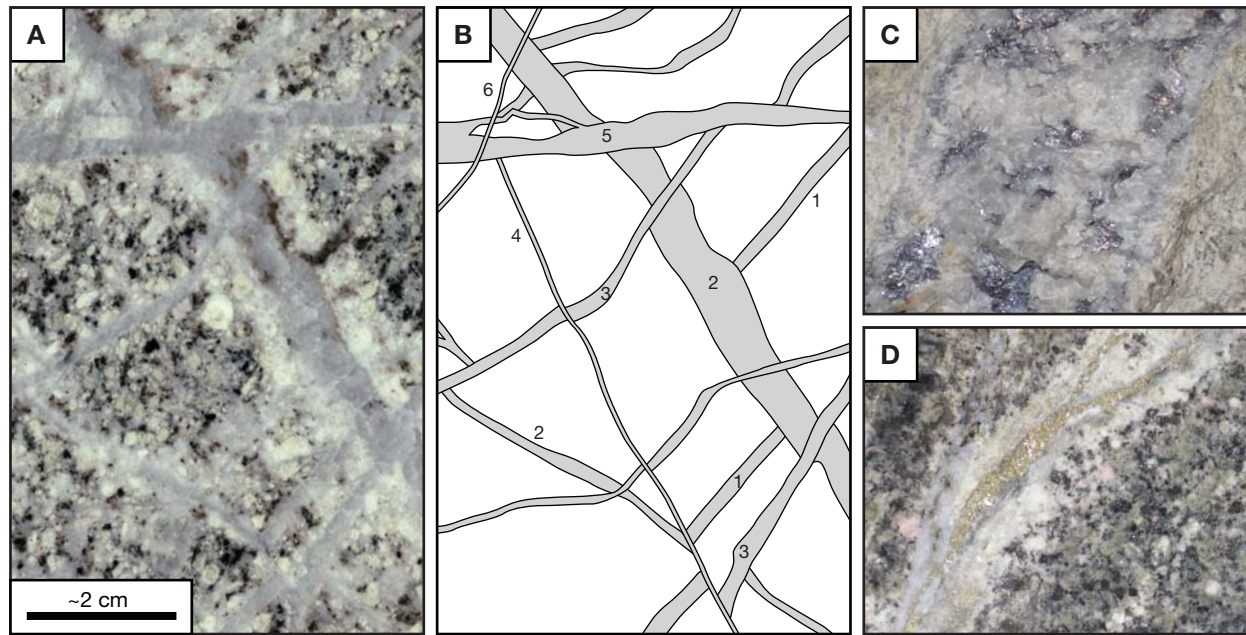


FIG. 4. Rock slabs showing the three major types of hydrothermal veins, with some timing relationships. A. Multiple quartz stockwork veins in QMP. B. Sketch of crosscutting timing relationships in (A), with numbers indicating changes in vein orientations between crosscutting veins. C. Quartz-molybdenite vein in highly potassically altered LP. D. Quartz-pyrite vein with sericitic selvage cutting a thin quartz stockwork vein in previously altered equigranular monzonite.

redissolution, both within the quartz veins and in the potassically altered wall rocks. Potassium feldspar and biotite can occur in vein selvages (Redmond et al., 2001; Landtwing, 2004). Quartz stockwork veins are most intensely developed in the QMP, but vein truncations at intrusive contacts of later porphyries show that a similar sequence of vein formation was repeated with decreasing intensity after the emplacement of each porphyry intrusion (Redmond, 2002). Quartz stockwork veins postdating the late QLP are sparse, straight walled, and only weakly Cu mineralized; they commonly have restricted halos of biotite alteration.

Quartz-molybdenite veins and molybdenum distribution

Quartz-molybdenite veins (Fig. 4C): Quartz-molybdenite veins form a distinct later vein generation that consistently crosscuts all quartz stockwork veins and even the latest porphyry dikes (i.e., the QLP; Redmond and Einaudi, 2010). They commonly occur as single, laterally extensive (1–10 m) veins with straight walls that are at least 1 cm wide (sometimes up to 10 cm wide). In contrast to the quartz stockwork veins, the quartz-molybdenite veins are commonly symmetrical with free-standing euhedral quartz crystals in the center. Molybdenite occurs as a selvage mineral predating most quartz, as bands within the quartz, or as euhedral platelets overgrowing the quartz. Minor chalcopyrite in these veins predominantly occurs as late vug-filling crystals, bornite is absent. Quartz-molybdenite veins crosscut even the rare quartz stockwork veins in late QLP dikes. They are typically associated with biotite-stable alteration extending at least tens of centimeters away but lack potassium feldspar selvages.

Molybdenum distribution: The distribution of molybdenum is systematically zoned relative to copper distribution, as

indicated first by Atkinson and Einaudi (1978). Detailed reevaluation of molybdenum distribution including a recent drilling program by Kennecott Utah Copper (G. Austin, G. Ballantyne, pers. commun.) showed that the molybdenum ore shell (e.g. 0.08 wt % MoS₂ contours, Fig. 3C, E) overlaps with the Cu ore shell (0.35 wt % Cu contour) at its inner and lower rim but extends to greater depths. The initial MoS₂ content of the Cu ± Au ore mineralized only by quartz stockwork veins is not precisely known but was probably rather low. High-grade MoS₂ regions that also contain QLP dikes were found to contain abundant quartz-molybdenite veins crosscutting the late porphyry dikes. This observation indicates that MoS₂ is dominantly (estimated 60–90%) hosted by the distinctly late quartz-molybdenite veins. The similar distribution of Cu and MoS₂ grades is therefore surprising, given that quartz-molybdenite veins formed late in the cyclic history of porphyry intrusion and quartz vein formation, whereas most of the Cu deposition immediately follows the QMP and predates the later latite dikes.

Quartz-pyrite veins, feldspar-destructive alteration, and late Au mineralization

Feldspar-destructive alteration: A late-stage phyllitic to argillic overprint postdates potassic and propylitic alteration and is best developed at the northeastern and southwestern ends of the deposit, overprinting all dike types as well as sedimentary rocks (Lanier et al., 1978; Babcock et al., 1995; Parry et al., 2002; Redmond, 2002). Zones of this late hydrous alteration along the northwestern side of the Cu deposit coincide with and extend northeast and southwest from the QMP (Babcock et al., 1995). Its intensity increases upward above the central Au-Cu orebody (Redmond et al., 2001; Landtwing,

2004). Sericite is the most prominent mineral in the southwestern part of the equigranular monzonite and QMP, where it occurs in selvages around quartz-pyrite veinlets which occasionally coalesce into pervasive alteration. Illite, smectite and kaolinite replace plagioclase phenocrysts even in areas of dominant earlier biotite (Landtwing, 2004). More intense clay alteration with minor sericite occurs in and around the LP dikes along the northwestern part of the deposit, where it may overprint slightly earlier sericitic alteration.

Quartz-pyrite veins with sericitic selvages: Quartz-pyrite veins with sericitic selvages are generally thin (0.5–5 mm) and control the feldspar-destructive alteration (Fig. 4D). They occur in swarms and anastomosing fracture sets of mostly subvertical orientation (as described in more detail below). Quartz-pyrite veins with sericitic selvages contain pyrite as their dominant vein mineral, variably accompanied by quartz, calcite, and locally some chalcopyrite or late bornite, and correspond to “D veins” of Gustafson and Hunt (1975).

Vein Geometry and Distribution

The aim of this study was to obtain a quantitative measure of vein frequency (number of veins per linear interval, as a function of space in three dimensions), vein density (measured as vein volume percentage in rock), and vein orientation (dip and dip direction) for three main stages of veining (Fig. 4): (1) barren or mineralized quartz stockwork veins associated with potassic alteration in the inner zones or propylitic alteration in the periphery; (2) quartz-molybdenite veins; and (3) quartz-pyrite ± carbonate veins with bleached halos of feldspar-destructive alteration (herein referred to as quartz-pyrite veins). Quartz-filled “early dark micaceous” veins (EDM, Redmond and Einaudi, 2010) were included with the quartz stockwork veins but never contributed appreciably to vein density. Some ambiguity arose where a quartz stockwork vein was reopened at the quartz-pyrite veins veining stage, as evident from bleached feldspar-destructive alteration surrounding otherwise massive quartz-dominated veins; clear cases were counted as quartz stockwork veins.

Data acquisition

In total 51 intervals, including drill core and mine bench faces, were measured and documented in detail by Gruen (2007). Vein orientations could only be recorded for surface intervals, for lack of oriented drill cores. See Appendix for details of data transformation, graphical representation, and statistical analysis.

Subsurface measurements were carried out on 15 drill core intervals of 5- to 14-m length (rarely 3–5 m in cores with high

vein density). For each vein, the apparent thickness between vein walls was measured in the direction of the core axis (Fig. 5), in order to obtain a measure of the volume fraction of vein material in the rock, irrespective of variable vein orientation. By summing up all apparent vein thicknesses of each of the three vein types and dividing the sums by the total length of a core interval, we obtained an estimate of the volumetric portion of each vein type in percent, which we here call vein density. In addition, vein frequency was measured by counting the number of veins of each type, divided by the interval length.

Mine bench exposures were mapped at 36 locations, systematically following a horizontal line (“scanline”) defined by extending a string along a segment of the pit wall. Depending on the accessibility of the bench walls, mapped segment lengths ranged from 2 to 6 m (rarely 1–2 m in areas of high vein density). Care was taken to select an interval that is representative for at least 10 to 20 m of surrounding pit wall. Apparent vein thicknesses were measured by projection onto the scanline to get a volume estimate, comparable to that in drill core. In addition to measurements of vein density and frequency, the orientation of each vein was measured and recorded with supplementary information about rock types and mineralogy using a simplified “Anaconda” mapping method (Einaudi, 1997, 2000). Vein orientations were recorded as dip direction and dip of vein planes relative to True North (local magnetic declination at time of data acquisition (2006) was ~12.5° E).

Vein orientation

Orientation measurements of veins and their abundance at the pit surface are summarized in stereograms of Figure 6. Quartz stockwork veins are the most abundant vein type. Their poles (red dots, Fig. 6A) predominantly lie along a great circle which dips ~30° to the southeast. Quartz-molybdenite veins are less frequent than the other vein types. Their orientations (blue triangles, Fig. 6A) are more scattered, and it is therefore difficult to identify a preferred direction. Quartz-pyrite veins with sericitic selvages are dominantly steep (green crosses, Fig. 6A, see also Fig. 6C) and show a preferred strike direction, which is seen more clearly in the rose diagrams of Figure 7. Here, the quartz-pyrite veins from adjacent mapping areas were grouped into five peripheral sectors to gain better statistical significance. As already observed in Figure 6A, quartz-pyrite veins were observed mainly in sedimentary rocks outside the southwestern and northeastern terminations of the QMP. Their strikes tend to point radially, in a fanlike manner, toward the center of the pit (see also Fig. 7).

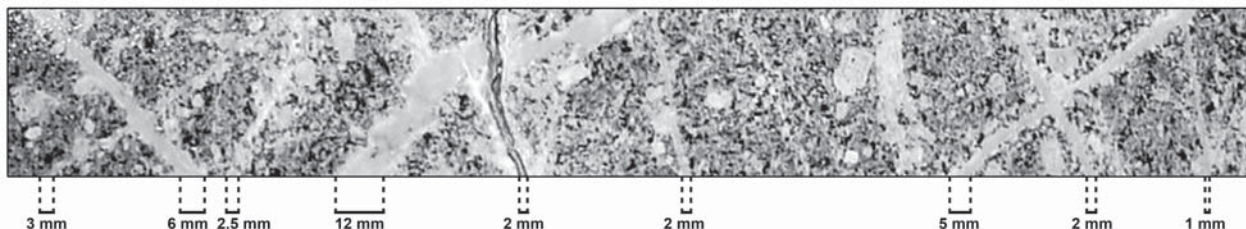


FIG. 5. Photograph of a QMP drill core to explain the principle of measuring apparent vein thicknesses to obtain volumetric vein density estimates for a chosen profile interval.

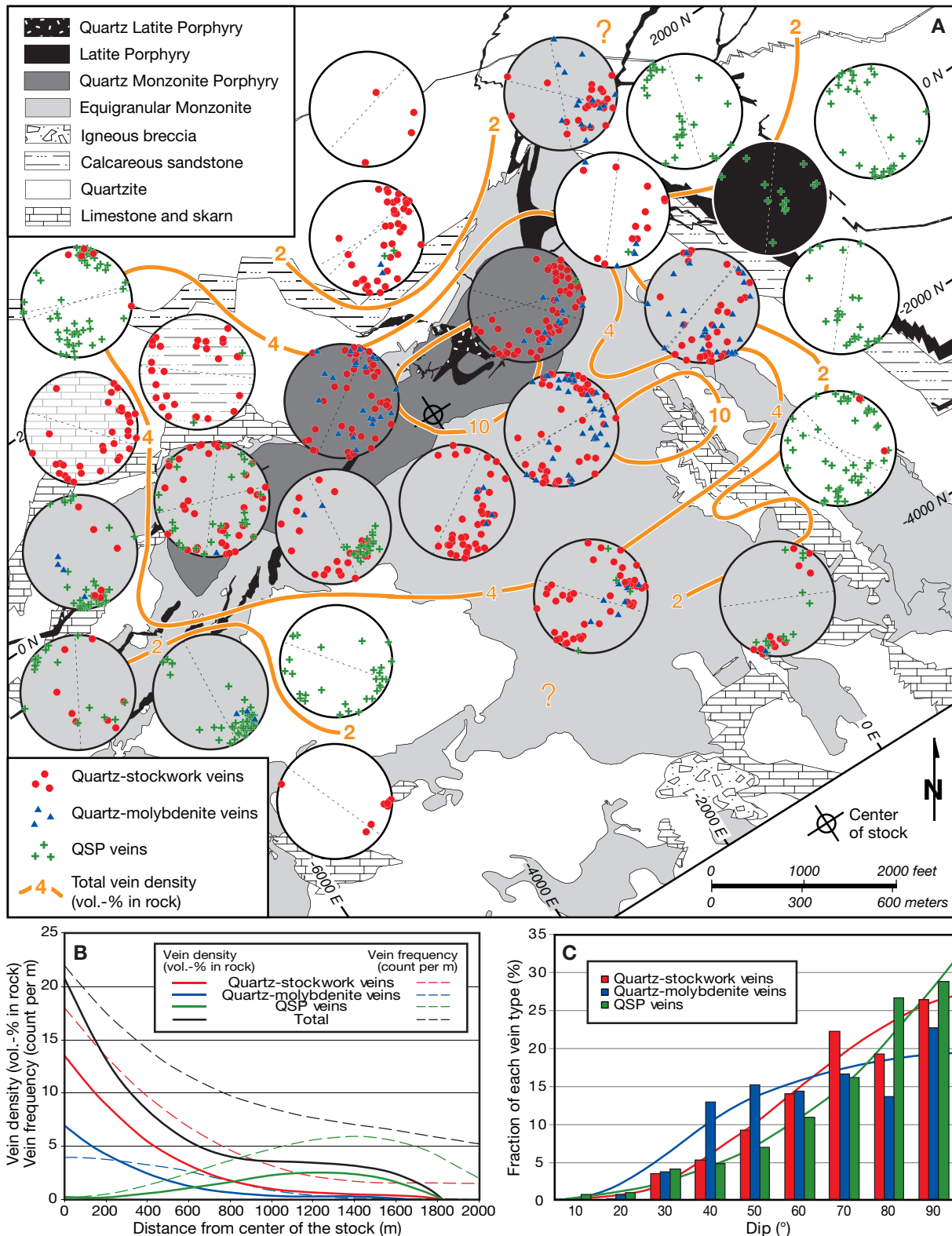


FIG. 6. Summary of surface measurements. Orientations are relative to True North. A. Simplified geologic map showing equal area Schmidt nets of the lower hemisphere for poles to veins measured along mine benches, together with manually drawn vein density contours (orange lines; in vol % total veins). Fill patterns of stereonets correspond to host lithologic units; a few adjacent locations were grouped. Vein types are distinguished by circles, crosses, and triangles. Orientations of scan-lines are indicated with thin dashed lines. B. Separate and integrated surface vein densities (vol %) and frequencies (count per 1 m of interval) for the three vein types as a function of distance from the center of the QMP stock (-220N/-2220E mine coordinates). C. Dip histogram of the same three vein types. QSP veins = quartz-pyrite veins with sericitic alteration halos.

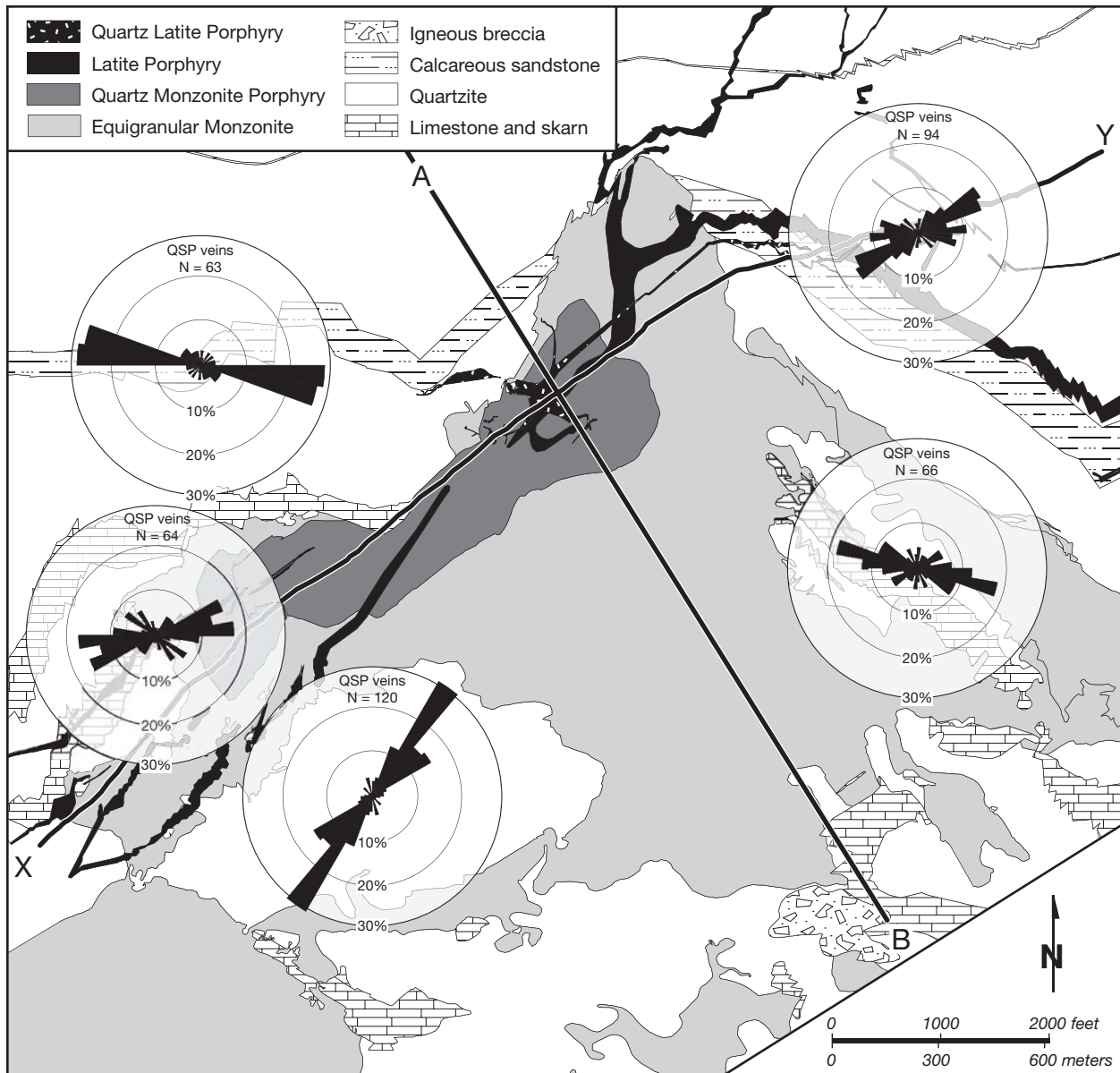


FIG. 7. Simplified geologic map with rose diagrams showing strikes of the quartz-pyrite veins with sericitic alteration halos (QSP veins), roughly grouped by location around the center of the pit. Thick black lines indicate surface traces of the two cross sections A-B and X-Y (Figs. 3, 10).

A bias in orientation measurements along a scanline could result from the tendency to overlook veins with strikes parallel to the scanline (i.e., parallel to the mine bench). To account for such a potential bias, the orientation of the scanline for each bench mapping location is indicated as a dashed line in the stereoplots of Figure 6A. Most of the stereoplots show veins striking both parallel and at variable angles to the scanline (i.e., vein poles do not cluster around tips of the dashed lines). This indicates that the bias in orientation data is not substantial.

The stereonets in Figure 8 plot the orientations of all three vein types without respect to their location within the pit but contoured for directional frequency. Each of the three stereoplots on the left-hand side shows vein poles

relative to True North and present-day vertical coordinate system, as measured in the field. For the plots on the right-hand side of Figure 8, the entire dataset was rotated 25° westward around a horizontal axis pointing to N 58° E. This rotation axis is oriented parallel to the largest horizontal extent of the QMP in map view (Fig. 2). The inclined southwest-northeast cross section (X-Y) introduced in Figure 8D and E represents the plane defined by this rotation axis and the direction of longest dimension of the QMP (based on three-dimensional geometric modeling of Kennecott Utah Copper data). Our rotation therefore reorients the recorded data, together with the cross section X-Y, into an inclined coordinate system defined by the principal axes of the QMP. This coordinate system may not have been precisely vertical

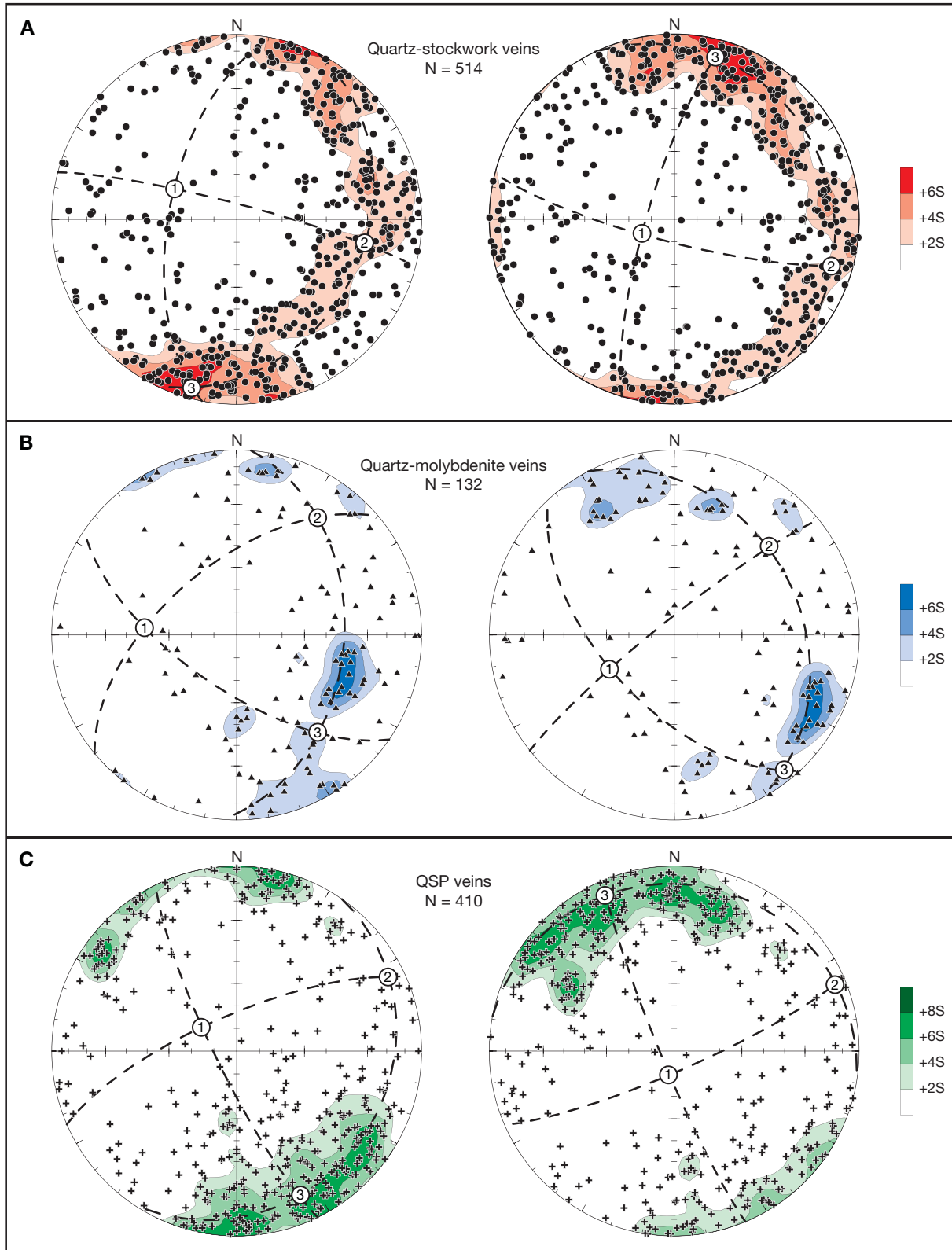


FIG. 8. Vein orientations plotted as poles in equal area Schmidt nets of the lower hemisphere, separated by vein type. A. Quartz stockwork veins. B. Quartz-molybdenite veins. C. Quartz-pyrite veins with sericitic selvages (QSP veins). Plots on left are data as measured in the field, plots on right are rotated 25° westward around a horizontal axis pointing to N 58° E. Outlined numbers indicate the minimal [1], intermediate [2], and maximal [3] principal directions, representing the least, intermediate, and highest accumulation of data points, respectively. Contour levels are in multiples of the standard deviation S above the expected count (refer to Appendix for a more detailed description of statistical analysis).

at the time of emplacement and vein formation, but structural reconstruction based on volcanic stratigraphy indicates that the porphyry body was emplaced with a distinctly steeper plunge prior to extension-related block tilting.

The following observations refer to the rotated data on the right-hand side of Figure 8 as our best estimate of true orientations at the time of vein formation. Directional statistics (see App.) yields point-density contours and three principal pole directions [1], [2], and [3], representing the least, intermediate, and highest accumulation of data points, respectively.

The poles of the quartz stockwork veins (Fig. 8A) lie in a great circle with shallow dip ($\sim 15^\circ$ NE), which corresponds to steeply oriented veins with variable strike direction. While the maximal [3] and intermediate [2] principal pole directions could be interchanging or rotating within a subhorizontal plane, the minimal principal pole direction [1] has a distinct, nearly vertical plunge. The quartz-molybdenite vein poles (Fig. 8B) form clusters along a rather weakly developed great circle with moderate dip ($\sim 30^\circ$ NE). A preferred orientation of veins is therefore not identifiable. The poles of quartz-pyrite veins (Fig. 8C) show a distinct cluster, elongated along a moderately developed great circle with subhorizontal dip and indicating the presence of steep veins striking preferably northeast to east.

Volumetric vein distribution

While Figure 6A shows contours of total vein density in volume percent (vol %) per rock, in Figure 9, vein densities of the three different vein types are plotted separately, in correlation with ore grades. Within an area of about 1×2 km 2 centered in the QMP intrusion, total vein density exceeds 4 vol percent, locally rising to >10 vol percent in the center (Fig. 6A). Throughout this region, vein density is dominated by quartz stockwork veins (>50% of total vein volume; Fig. 6B). Quartz stockwork veins represent the pathways for Cu and Au mineralization, and their distribution outside the barren core zone correlates well with the zones of high Cu ore grade (Fig. 9A). Quartz-molybdenite veins contribute to less than 30 percent of total vein volume (Fig. 6B). Similar to quartz stockwork veins, quartz-molybdenite veins also show highest values within the QMP. Their overall distribution correlates even more closely with the MoS₂ grade (Fig. 9B). In the periphery of the deposit, total vein density rapidly drops off to 2 vol percent or less (Fig. 6A), and quartz-pyrite veins become the most frequent vein type (Fig. 6B). They show a different distribution pattern and do not correlate with any of the high-grade ore zones but rather form two areas of high density outside the two ends of the thick QMP dike (Fig. 9C).

Volumetric vein density measurements at the pit surface were combined with drill core data to extend the contours into the more recently mined Au-Cu-rich orebody in the lower part of the open pit. Vein density values measured along mine benches generally turned out to be somewhat higher than the ones from core logging in adjacent areas. This apparent systematic overestimation along mine benches may result from different rock conditions—in drill holes, the rock material is well preserved and cleancut, whereas in mine

benches it is fractured and has an irregular surface. Similar to observations at the pit surface, total vein density along the subsurface part of the two cross sections is dominated by quartz stockwork veins.

Total vein densities were analyzed along the two profiles A-B and X-Y (Fig. 10). The vertical section at -1400E (mine coordinates) cuts at right angle across the QMP intrusion (Fig. 10A). Figure 10B is oriented through the center of the open pit along a plane dipping 65° toward N 32° W, following the assumed emplacement direction of the QMP. Both sections show similar distribution patterns, though in the long section X-Y they appear broader. The highest total vein density (>8 vol %) occurs in the center and along the footwall of the QMP. High densities of >4 vol percent quartz stockwork veining occupy a broad area, extending into the adjacent equigranular monzonite and below the entire cup-shaped Cu orebody. This observation is consistent with results from a companion study at a more detailed scale (5–10 vol % veins within QMP and equigranular monzonite; Redmond and Einaudi, 2010). Even higher vein densities (>20 vol %) were locally recorded at the surface of the pit. It is noticeable that even with depth, despite a rapid drop-off of Cu ore grade, relatively high vein densities continue within the QMP, as shown by both sections (Redmond and Einaudi, 2010). South of the QMP, within the equigranular monzonite, the intervals between neighboring contour lines are wider, compared to the northern side where the QMP is in contact with sedimentary host rocks and vein densities show a sharp gradient. Typical vein densities in sedimentary rock, even if well mineralized, are generally smaller than 2 vol percent; in comparison to measurements within the equigranular monzonite, which lie between 4 and 6 vol percent over a broad zone. Density contours are shown to close in the upper part of the orebody, based on a small number of observations of old (~1960) core intersections above the present pit outline. While an upward decrease of quartz vein density is obvious from these intersections, the contours have to be treated as rough interpolations only.

Discussion and Interpretation

The mine-scale distribution of vein abundance, density, and orientation in successive geologic stages of the Bingham Canyon deposit can be interpreted in terms of changing fluid pressure and differential stress¹ in an evolving magmatic-hydrothermal system (Nakamura, 1977; Delaney et al., 1986; Jolly and Sanderson, 1997; André et al., 2001; Tosdal and Richards, 2001; Stephens et al., 2004). Our interpretation attempts to explain more generally the preponderance of steep structures, including magmatic contacts as well as hydrothermal veins, which is typical for the depositional environment of many porphyry-style ore systems (e.g., Heidrick and Titley, 1982; Carten et al., 1988; Tosdal and Richards, 2001; Stephens et al., 2004), in contrast to the prevailing flat structures in deep plutons and related veins. The discussion first addresses the rock mechanics significance of preferred vein orientations. We then

¹ In this study, σ_1 is the maximum compressive principal stress, whereas σ_3 is the minimum compressive principal stress. σ_2 is the intermediate principal stress; therefore $\sigma_1 > \sigma_2 > \sigma_3$.

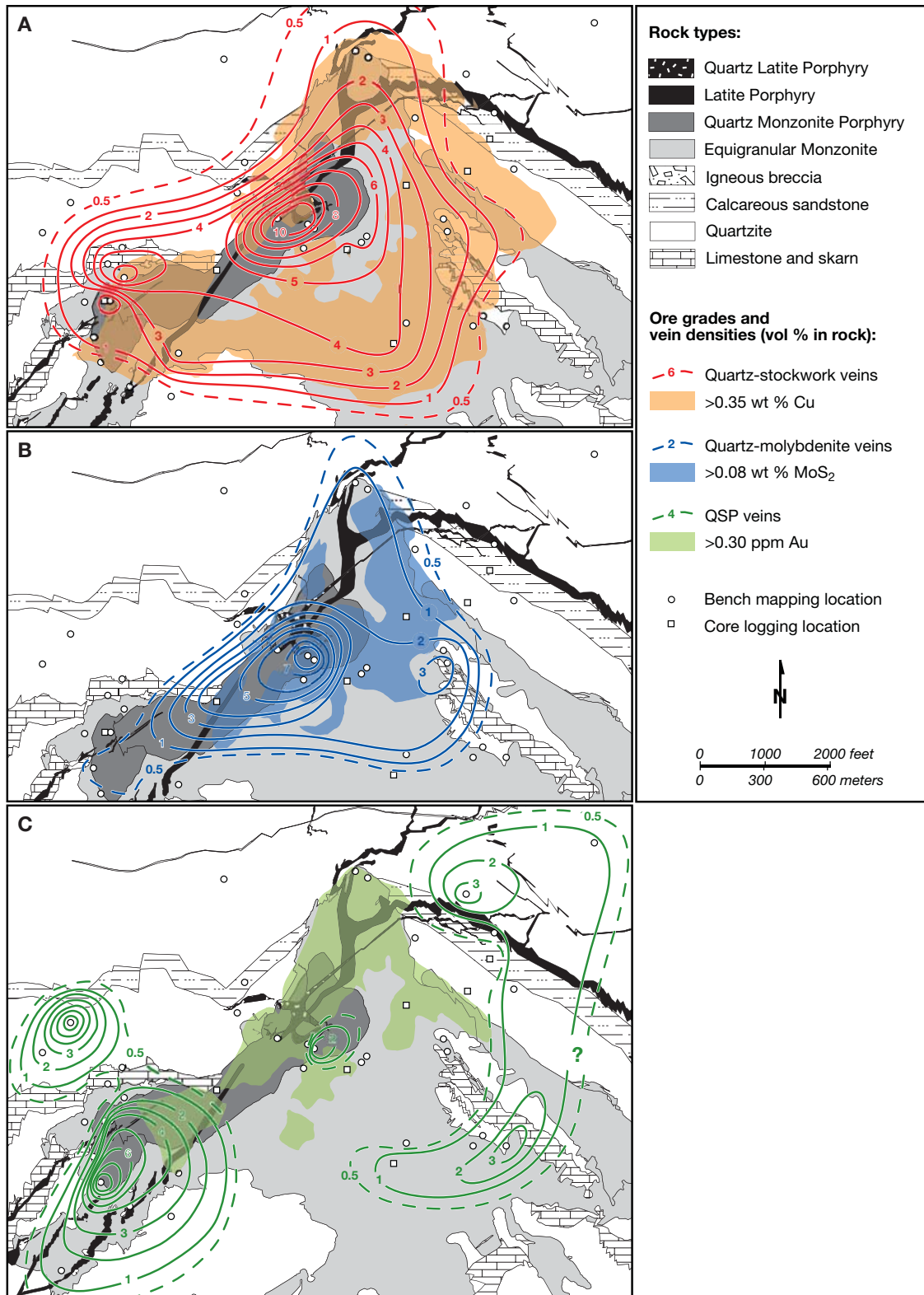


FIG. 9. Simplified geologic maps showing vein density contours in vol percent for the three major vein types, together with ore-grade contours and stations of surface mapping (circles) and core logging (squares) locations. A. Quartz stockwork vein density contours highly overlap with the >0.35 wt percent Cu ore grade and show highest values (>7 vol %) within the QMP. B. Quartz-molybdenite vein densities, similar to quartz stockwork veins, show highest values (>4 vol %) within the QMP and correlate well with the >0.08 wt percent MoS₂ ore grade. C. Quartz-pyrite veins with sericitic alteration halos (QSP veins) are less abundant in the center of the pit but occur dominantly at the northeastern and southwestern edges of the deposit. They show no correlation to any of the ore grades.

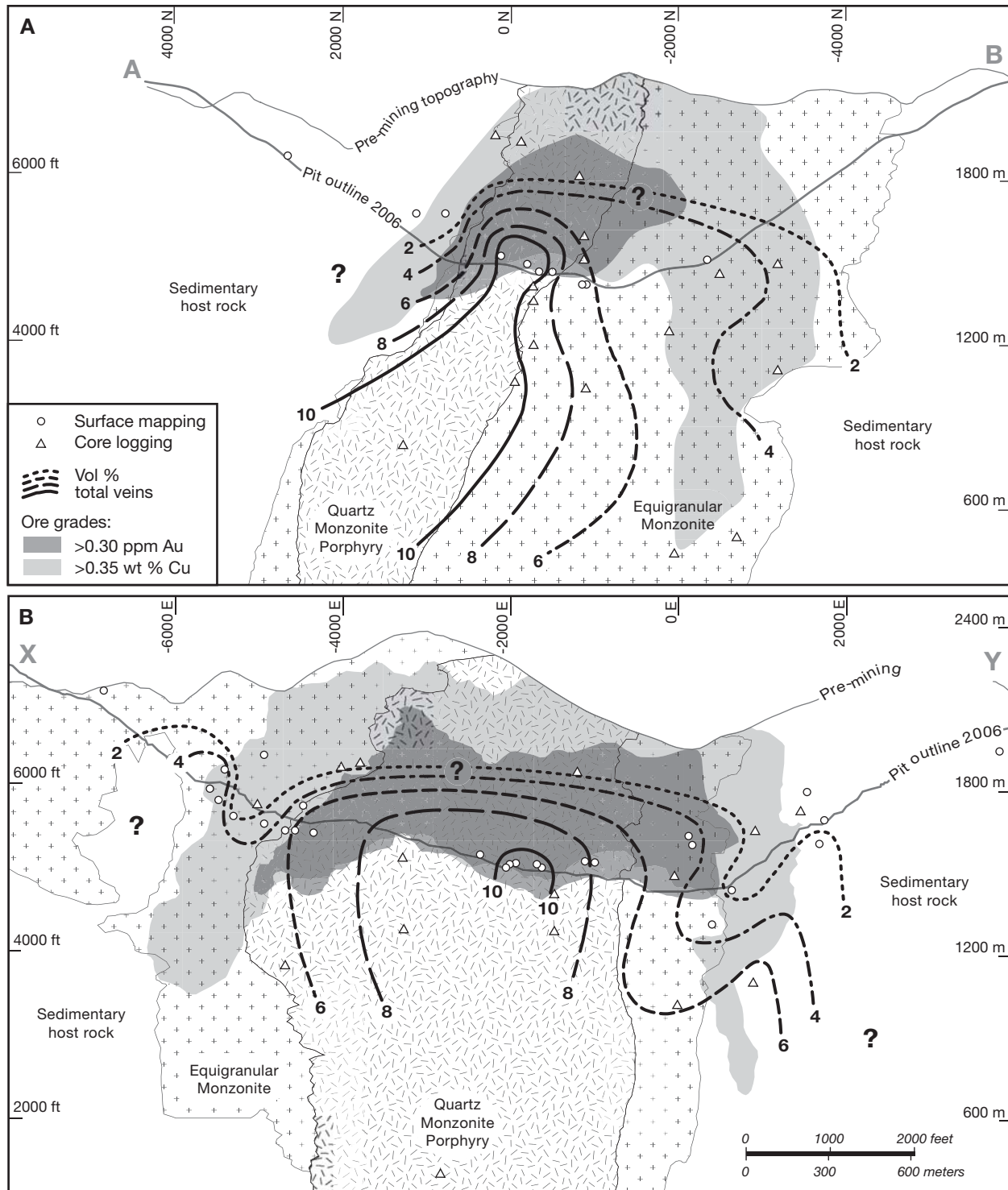


FIG. 10. Two geologic profiles showing vein density contours relative to lithologic units as well as ore grades of Cu and Au, indicating also projected surface mapping (circles) and core logging (triangles) locations. A. Northwest-southeast cross section (A-B). B. Southwest-northeast cross section, dipping 25° to the north-northwest (X-Y). Grid in mine coordinates (ft).

propose a sequence of events of magma-fluid-rock interaction, inspired by recent geodetic data of active volcanoes. Finally we conclude with a tentative interpretation of permeability evolution within the vein stockwork during Cu-Au and Mo mineralization.

Vein orientation, fluid pressure, and differential stress

The minimum compressive principal stress σ_3 determines the opening direction of a vein in a previously unfractured rock, such as a hydrous magma that just cooled below its solidus. In a rock mass already containing numerous fractures

of variable orientation, a pure extension vein will open where the minimum compressive principal stress σ_3 is oriented perpendicular to a fracture. However, vein formation occurs more easily by shear failure, because fluid pressure reduces the frictional resistance to slip on any existing fracture surface (Townend and Zoback, 2000; Cox et al., 2001). In this case, individual vein walls can be oblique to σ_3 , but, on average among many veins, the favored direction of opening still corresponds to the direction of σ_3 . The two larger principal stress directions σ_1 and σ_2 will be in the plane of a pure extension vein and parallel to the majority of veins in a large array of opening fractures. Predominantly steep veins with variable strikes (poles on a great circle) therefore indicate a common subvertical σ_1 orientation (Fig. 8). However, the statistically determined principal directions of highest [3] and intermediate [2] concentration of data points do not necessarily correspond to a static differential stress of subhorizontal σ_3 and σ_2 directions. Instead, the variation of strike directions with a predominantly subvertical dip indicates that σ_3 and σ_2 were either subequal or rotated in a subhorizontal plane. The latter is consistent with mutual crosscutting relationships (Fig. 4B) and the observation in other porphyry deposits of intersecting concentric and radial vein arrays (Carten et al., 1988; Tosdal and Richards, 2001; Cannell et al., 2005).

Alternating stages of magma intrusion and vein formation

Recent geodetic data from areas of active magmatism provide new insights into the mechanisms of subsurface magma emplacement and fluid expulsion from hydrous intrusions into upper-crustal hydrothermal systems. Intrusion of volatile-rich magmas leads to cycles of uplift and domal extension, alternating with depression and contraction of caldera roofs (Bonafede, 1991; Todesco et al., 2004; Hurwitz et al., 2007; Hutnak et al., 2009). Numerical modeling of geometry and timescale of these ground-surface displacements indicates

transient injection of overpressured, presumably magmatic fluids to shallow depths of <3 km below surface, well above the depth of the actual intrusion roof (Todesco et al., 2004; Bodnar et al., 2007; Hurwitz et al., 2007). Fluid expansion across the transition from lithostatic to hydrostatic pressures can lead to phase separation, which further enhances updoming and local extension, before the deep fluids eventually drain into the ground-water regime over periods of months to years (Cappa et al., 2009; Hutnak et al., 2009; Lima et al., 2009). The steep gradients in temperature, fluid pressure, and fluid phase state implied by such rapid variations in active systems are consistent with large pressure fluctuations recorded by fluid inclusions in exposed porphyry-style ore deposits and with rapid and voluminous fluid flow as required for ore formation. Recorded pressure fluctuations between distinct inclusion assemblages, even in a single vein, can approach or exceed the difference between lithostatic and hydrostatic pressure (e.g., Audébat et al., 1998; Ulrich et al., 2001; Redmond et al., 2004).

A physical interpretation of alternating intrusion and veining stages at Bingham Canyon must explain the observed predominance of steep veins and intrusive dikes, as well as the subordinate but common occurrence of otherwise identical vein and dike segments with some flat or gently dipping orientations in all stages. It must also explain the preferred southwest-northeast orientation of structural elements in some stages, alternating with variable strike directions of subvertical vein structures in other stages. These observations may be explained by a cyclic interplay between two regimes of fluid pressure and differential stress in the roof of an inferred magma chamber, which drives the subvolcanic magmatic-hydrothermal system from greater depth (Fig. 11; cf. Cannell et al., 2005).

A. An asymmetric transtensional regime of overall small differential stresses, in which northeast-striking steep fractures

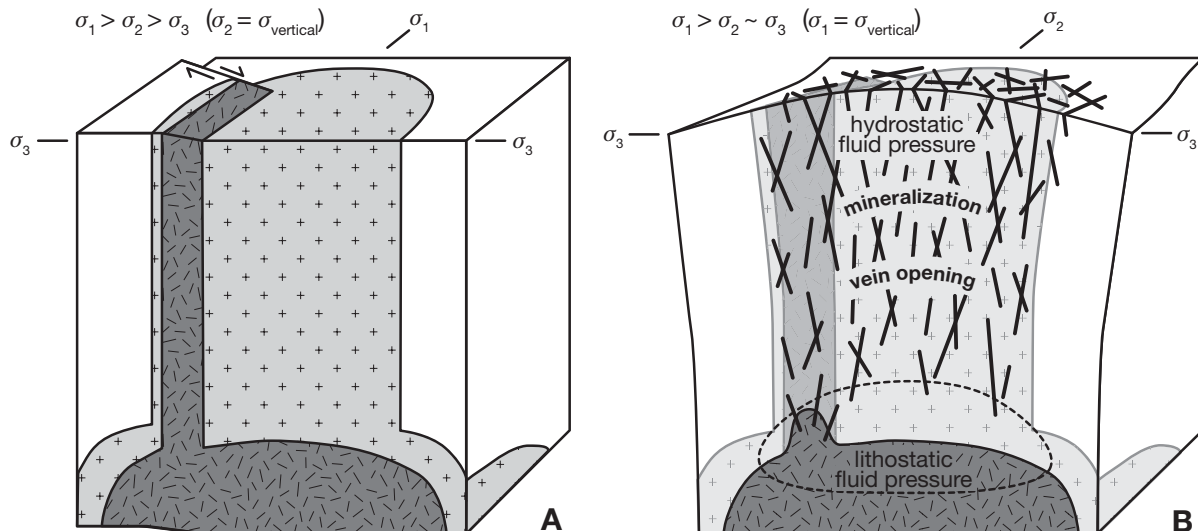


FIG. 11. Block diagrams illustrating the two end-member stress states of the magmatic-hydrothermal system. A. Asymmetric transtensional regime where opening of jogs and emplacement of intrusions take place. B. Symmetric extensional regime with subvertical σ_1 and subhorizontal $\sigma_2 \sim \sigma_3$ caused by roof bulging and radial extension due to underlying fluid overpressure. The resulting extensional vein stockwork, forming well above the magmatic front and the lithostatic to hydrostatic transition, is likely to be a key to metal accumulation in high-grade porphyry ore shells.

are opened dominantly by shear failure. It has a stable component of horizontal stress differences, with σ_1 directed approximately southwest-northeast and σ_2 in near-vertical orientation.

B. A radial extension regime with subvertical σ_1 and significantly smaller but similar $\sigma_2 \sim \sigma_3$, forming multiply intersecting steep stockwork veins as a result of σ_2 and σ_3 fluctuating in subhorizontal directions. Radial extension is proposed to result from upward bulging of the ore shell region by the underlying region of magmatic fluid overpressure and the roof of the magma chamber itself. In this environment, vein formation not only occurs by hydraulic fracturing (i.e., driven by reduction of effective stress) but primarily by rock extension well above a deep and broad high-pressure region (i.e., by an increase of differential stress).

Alternating stress states between these two end-member regimes can explain the observed sequence of stages during the formation of the Bingham Canyon deposit (Fig. 12):

Stage 1—emplACEMENT of the equigranular monzonite, comprising several dikes and stocks with variable contact orientations, which may follow regional structures (Einaudi, 1992). The equidimensional outcrop area and steep walls of the equigranular monzonite (Fig. 2) indicate that its emplacement is controlled by lateral extension in varying directions (as reconstructed by J. Grocott and A. Kloppenborg, pers. commun.; Fig. 12-1) and an unknown fraction of vertical mass displacement, including stoping of large exposed sediment rafts and roof lifting above the present erosion surface. We infer that this stage was mechanically dominated by the magma supply to a much larger, deeper seated magma chamber. This caused roof extension and established regime B for the first time, still without large-volume fluid saturation. This stage probably included the build-up of the overlying volcanic edifice, as roof doming would favor the opening of feeder dikes above the equigranular monzonite stock.

Stage 2—emplACEMENT of the thick QMP dike—was localized by the far-field stress activating preexisting faults in the sedimentary rocks (asymmetric stress regime A; Fig. 11A). The vertically elongated box shape of the QMP (Figs. 2, 3) necessitates a component of shear displacement along steep faults, i.e., with a σ_3 oriented roughly northwest-southeast and σ_1 approximately southwest-northeast (Fig. 12-2). The bounding shears have not been mapped but could belong to the prominent family of north-northwest-trending faults in the central part of the pit that cut the equigranular monzonite and also cause jogs in the later porphyry dikes (Fig. 2). Intrusion of the QMP along the northeast-oriented northern contact of the massive equigranular monzonite may have occurred at a time when this stock and the outer carapace of the subjacent magma chamber were already solidified and therefore able to transmit the far-field transtensional stress. The QMP magma may have originated from the interior part of the crystallizing magma chamber, in a geometric relationship resembling the deeply exposed Yerington batholith (Dilles, 1987).

Stage 3—main Cu-Au stockwork vein formation. Quartz-stockwork vein formation immediately followed the emplacement of the QMP, after the intrusion had released the differential regional stress field and high fluid pressure from below subjected the composite stock to symmetric tensional up-doming (stress regime B, Figs. 11B and 12-3). Hydraulic

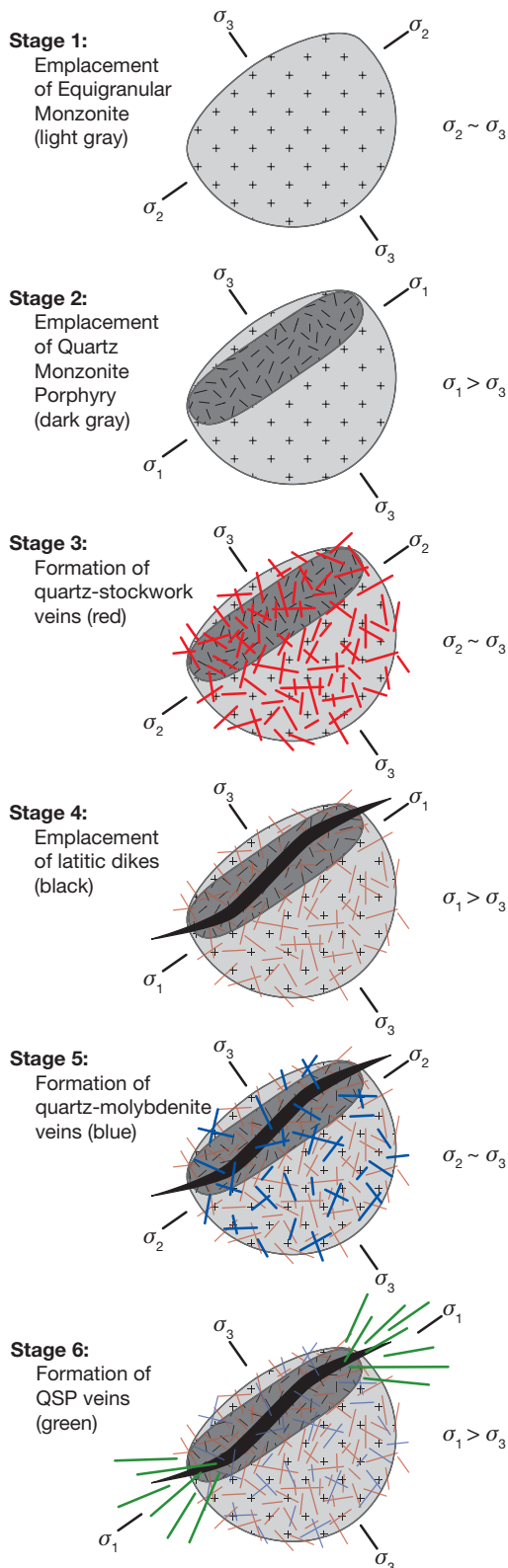


FIG. 12. Plan view sketches illustrating the time sequence of intrusion emplacement and vein formation at the Bingham Canyon deposit. Indicated are schematic geometry of intrusions, distribution and orientation of veins, and idealized local stress regimes when horizontal stresses were nearly subequal ($\sigma_2 \sim \sigma_3$; stages 1, 3, and 5) and a significant differential horizontal stress existed ($\sigma_1 > \sigma_3$; stages 2, 4, and 6).

fracturing is most intense in the QMP itself but extends in a roughly circular area into the equigranular monzonite (Fig. 9A). As detailed below (Fig. 13), the vein opening occurred in multiple cycles, starting with extensional failure at near-lithostatic fluid pressure and then evolving toward shear reactivation while veins are being filled with quartz and texturally later ore minerals.

Stage 4—emplacement of the laticic dikes, followed by renewed stockwork veins—encompassed at least two events of return to dominantly northeast-oriented dike emplacement in stress state A after the deep fluid overpressure was temporarily released by fluid drainage through the vein network related to the QMP, and after mineral precipitation had healed the rocks to allow transfer of far-field stress (Fig. 12-4). Each dike event was followed by repeated vein formation, driven by fluid overpressure that had built up in the magma chamber at depth (stress state B; Fig. 11B).

Stage 5—quartz-molybdenite veins reflect the last return to symmetrically extensional conditions of stress state B (Figs. 11B, 12-5), characterized by a sparser set of larger veins with dominantly steep but commonly also flat orientations. Vertically extensive MoS₂-rich zones at depth (Fig. 3E)

may reflect vein emplacement into an already quite cool and brittle, thoroughly prefractionated rock mass, by a last event of deep fluid-pressure buildup without related magmas reaching the present level of exposure.

Stage 6—quartz-pyrite veins with preferred southwest-northeast orientation reflect the return to the prevailing regional stress state A during the waning of the hydrothermal system (Fig. 12-6). As magmatic fluid pressure dissipated and hydrothermal heat advection decreased, the crust returned to its normal state of high crustal strength close to shear failure and moderately high permeability at near-hydrostatic conditions (Townend and Zoback, 2000). The concentration of steep quartz-pyrite veins along the northeastern and southwestern extensions of the QMP probably relates to local stress concentrations around a relatively competent body.

Permeability evolution, vein mineralization, and the origin of porphyry ore shells

The formation of a porphyry vein stockwork involves fracture formation as well as hydrothermal minerals infilling. This process can be understood by considering the structural and mineral zoning data in conjunction with textural observations and fluid inclusion data (Redmond et al., 2004; Landtwing et al., 2010). A new way of depicting the relationships of relative fluid pressure and rock stress was introduced by Cox (in press), as illustrated in Figure 13. The diagram plots fluid pressure normalized to vertical rock pressure on the vertical axis, i.e., attaining a value of 1 at lithostatic fluid pressure conditions where fluid pressure P_f equals the pressure determined by the weight of the overlying rock column. The horizontal axis shows the differential stress $\sigma_1 - \sigma_3$ irrespective of their orientation. The limits of rock failure are shown by a failure envelope with two segments: a segment at high fluid pressure and low differential stress where failure occurs by pure extension (red); and a segment at lower pore pressure but higher differential stress where failure occurs by shear displacement (blue). The position of the failure envelope expressed in these two variables depends strongly on depth below surface. The curve in Figure 13 is calculated for 2 km (the estimated depth of the center of the orebody), for typical properties of crystalline rocks and assumptions detailed in Cox (in press).

Based on the preceding discussion, we interpret that the normal state of the crust at Bingham Canyon was dominated by a small, regionally imposed difference between horizontal σ_1 and σ_3 , i.e., a transtensional situation with overall low differential stress consistent with point (1) in Figure 13. A cycle of dike emplacement and subsequent veining starts with magma pressure overcoming the regional stress field above a deep magma chamber, thereby opening a vertical extension jog in the direction of easiest major space creation (Fig. 11A). The dike is emplaced in the forefront of a deep and much broader zone of massive fluid pressure buildup in the roof of the subjacent magma chamber. Upward transmission of this fluid pressure is shown by the arrow (2) in Figure 13 and leads to extensional hydraulic fracturing in the roof of the magma chamber (Fig. 11B), including the preexisting equigranular monzonite in the deep core of the ore system, at point (3A). The porphyry magma itself exsolves a small amount of fluid upon crystallization, causing particularly

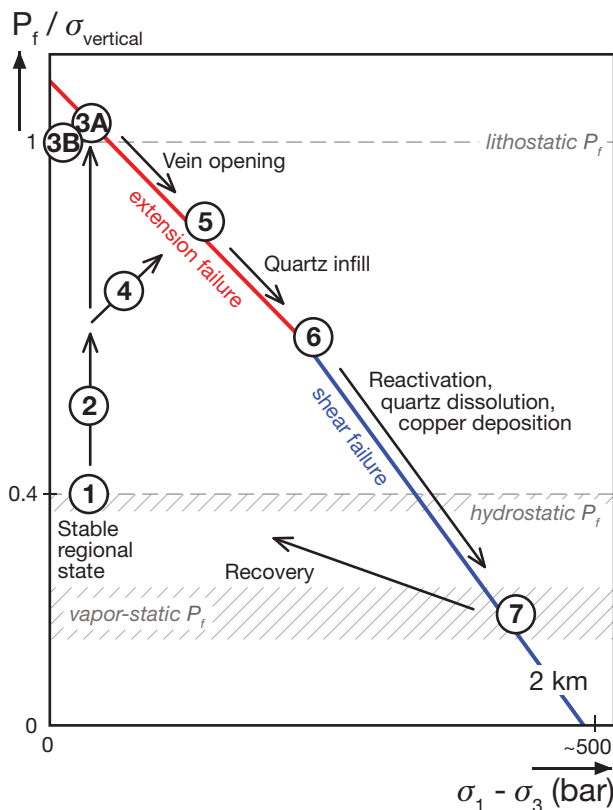


FIG. 13. Failure mode diagram for an extensional tectonic regime at crustal depth of 2 km, based on calculations from Cox (in press), indicating a possible stress and fluid pressure evolution path of the Bingham Canyon deposit. 1 = regional transtensional stress state; 2 = buildup of fluid pressure by fluids exsolving from a magma chamber; 3 = hydraulic fracturing of preexisting porphyry (A) and cooling pluton (B); 4 = simultaneous increase in fluid pressure and differential stress due to rock uplift and extension; 5 = vein opening by extension failure; 6 = transition toward shear failure; 7 = vein reactivation at vapor-static conditions.

intense local hydrofracturing at lithostatic condition and very small differential stress, because the fresh magma has just crossed its solidus, resulting in local fluid phase exsolution and an associated net volume expansion (Burnham, 1979; point (3B), Fig. 13). The pressure front from the large underlying fluid reservoir causes active rock uplift and radial extension (Fig. 11B) over a much wider zone than the QMP, on the scale of the 3-km broad ore shell or even beyond. Such radial roof extension causes an increase in differential stress, because it decreases both horizontal stresses σ_2 and σ_3 to a common low value, while σ_1 remains constant due to the weight of the overlying rock. Almost at the same time, the fluid pressure front advances into the region of the future orebody, leading to paths such as (4) in Figure 13. Observations of vein shapes described in this paper (Fig. 4A) and other porphyry copper literature indicate that most quartz stockwork veins form by extensional failure, implying that initial vein opening occurred at high (but depending on depth not necessarily lithostatic) fluid pressure, e.g., at points near (5) in the red failure segment of Figure 13. Once a fracture forms, parting of the crack walls will cause a fluid pressure reduction as the fluid expands into the open space. On the scale of the entire ore shell, however, the deep fluid overpressure is maintained, allowing continued extension and repeated cracking and vein formation. Despite overall falling fluid pressures, as the fluid drains upward, differential stress can therefore increase due to continued lateral extension of the rock column.

Upward draining of a dense fluid from the higher pressure region below causes every fluid aliquot to expand and cool adiabatically, leading to quartz precipitation and infill of open vein space. With continued pressure decrease, a region of the ore shell will evolve toward lower fluid pressure where opening becomes easier by shear failure (steeper, blue part of the failure curve in Fig. 13). This evolution toward point (6) explains some key features of the ore veins, documented in the companion paper of Landtwing et al. (2010). Cathodoluminescence petrography of stockwork veins at Bingham Canyon and other porphyry deposits (Rusk and Reed, 2002; Redmond et al., 2004; Klemm et al., 2007) shows widespread evidence for microfracture reactivation within previously filled stockwork quartz veins associated with redissolution of existing quartz. Based on fluid inclusion data, this occurs at low fluid pressure (<250 bars) where quartz solubility is retrograde (Fournier, 1983). The process helps to maintain high permeability for the precipitation of texturally late ore minerals into this new pore space. The proposed vein evolution path from (3) through (5) and (6) to (7) is consistent with fluid inclusion evidence showing large variations in fluid pressure during quartz vein evolution, even exceeding the difference between lithostatic and cold hydrostatic pressure. Vapor-static pressures as low as 150 bars (indicated by point (7); Fig. 13) imply that the upper part of the ore system evolved toward a vapor plume, in which fluid pressure was determined by the integrated weight of hot fluid with low density (Landtwing et al., 2010). Within one mineralization event, the evolution of fluid pressure and differential stress up and down along paths (5)-(6)-(7) can be locally repeated many times, leading to the multiply crosscutting veins (Fig. 4B) that characterize porphyry copper deposits, whereby each vein may

form the characteristic internal reactivation texture shown by cathodoluminescence. On the mine scale, the region of ore deposition will be stabilized by a balance between the roof extension driven from below and the outflow of adiabatically cooling fluids at essentially hydrostatic pressure. The cup-shaped ore shell at Bingham Canyon (Fig. 10) is probably localized by a limited window of pressure and temperature conditions, in which metal precipitation is maximized (see Landtwing et al., 2005, 2010).

Once the deep pressure front is dissipated by fluid drainage, the system recovers by collapse and limited contraction as far as the added volume of vein mineral permits. The rock mass thereby relaxes toward the near-neutral stress state (1), in which the small far-field predominance of horizontal σ_1 over σ_3 prevails. At the same time, remaining pore space is filled by cooling aqueous fluid if the dynamic vapor plume had temporally created vapor-static conditions. The preferentially northeast-trending quartz-pyrite veins associated with feldspar-destructive alteration (Fig. 12-6) are interpreted to result from shear failure as a result of a last, waning stage of magmatic fluid pressure buildup, as the fluid source became exhausted and the solidus region of the magma chamber had retracted to greater depth.

Conclusions

Structural observations on the evolving dike and vein geometry of the Bingham Canyon Cu-Mo-Au system indicate that the typical concentrically zoned “ore shell” of porphyry-type ore deposits is a result of rock extension ahead of a broad fluid pressure front driven by a deep hydrous magma chamber. Key evidence is the broad vein network extending well beyond the apparently coeval porphyry stocks and dikes and the highly variable strike directions of predominantly steep mineralizing stockwork veins.

Our concept of pressure-driven wall-rock extension differs from the classical concept of Burnham (1979), according to which porphyry ore shells are generated primarily by hydraulic fracturing of the caprock of a stock or cupola in the roof of an intrusion, triggered by the positive volume change upon crystallization of hydrous melt to rock + fluid (Burnham and Ohmoto, 1980). Our concept also modifies the model of Fournier (1999), in which the fracturing front is primarily controlled by the brittle to ductile transition as a function of rock temperature. The latter does not match observations at Bingham Canyon, where the majority of multiple vein sets formed by brittle extensional fracturing. The model of fluid pressure-driven rock extension matches observations from areas of active magmatic-hydrothermal uplift (Bodnar et al., 2007) and geologic features of other big porphyry copper systems. For example, it may resolve the apparently conflicting views published on the giant copper deposits of central Chile. As the biggest of them all, El Teniente has every characteristic of a giant porphyry Cu-Mo deposit (Cannell et al., 2005; Klemm et al., 2007) but also shows clear evidence that exceptionally intense fracturing, potassic alteration, and high-grade Cu-Mo mineralization extended far beyond the likely zone of influence of comparatively small porphyry dikes and stocks (Skewes et al., 2002). This observation does not call for a special type of deposit but can be readily explained by extension above a broad fluid

pressure front, sourced in a large deep-seated intrusion as suggested by both Skewes et al. (2002) and Cannell et al. (2005). The model is also consistent with the very fast rate of porphyry mineralization estimated from alteration kinetics by Cathles and Shannon (2007).

The difference between pressure-driven wall-rock extension and previous concepts has economic significance for high-grade metal enrichment. The concepts of Burnham (1979) and Fournier (1999) predicted that the zone of ore deposition migrates downward as a result of overall cooling of a porphyry stock or a cupola in the roof of a magma chamber. This implies that an amount of ore metals contributed by a given amount of fluid would be "smeared out" over a considerable vertical distance, which reduces the final ore grade in the rock. By contrast, the site of vein formation and mineralization according to our concept can be stabilized in an almost stationary ore shell, by a dynamic balance between deep fluid pressure, the resulting domal or tube-shaped wall-rock extension, and drainage of the magmatic fluid upward and outward into the hydrostatic fluid domain.

Acknowledgments

This paper is the second in a series of papers, as part of an ongoing study of ore-forming magmatic-hydrothermal processes in the giant Bingham Canyon deposit. It would not have been possible without the collaboration with Kennecott Utah Copper (KUC), a subsidiary of Rio Tinto. Geoff Ballantyne, Gerry Austin, and the late Ricardo Presnell contributed actively in providing present mining data. Discussions with Thomas Driesner, Marco Einaudi, Stephen Cox, Larry Cathles, John Dilles, and Dick Tosdal gave important new insights. Special thanks to the Bingham Canyon geology staff and Bob Moore for kindly hosting, teaching, and guiding us at the mine. Comments by David Cooke, John Proffett, Stephen Cox, and an anonymous reviewer greatly helped to improve the paper. Continued financial support by ETH Zurich and the Swiss National Science Foundation (Project 200020-116693) is gratefully acknowledged.

REFERENCES

- André, A.S., Sausse, J., and Lespinasse, M., 2001, New approach for the quantification of paleostress magnitudes: Application to the Soultz vein system (Rhine graben, France): *Tectonophysics*, v. 336, p. 215–231.
- Annen, C., and Sparks, R.S.J., 2002, Effects of repetitive emplacement of basaltic intrusions on thermal evolution and melt generation in the crust: *Earth and Planetary Science Letters*, v. 203, p. 937–955.
- Atkinson, W.W., and Einaudi, M.T., 1978, Skarn formation and mineralization in contact aureole at Carr Fork, Bingham, Utah: *ECONOMIC GEOLOGY*, v. 73, p. 1326–1365.
- Audétat, A., Günther, D., and Heinrich, C.A., 1998, Formation of a magmatic-hydrothermal ore deposit: Insights with LA-ICP-MS analysis of fluid inclusions: *Science*, v. 279, p. 2091–2094.
- Babcock, R.C., Ballantyne, G.H., and Phillips, C.H., 1995, Summary of the geology of the Bingham District, Utah: *Arizona Geological Society Digest*, v. 20, p. 316–335.
- Beane, R.E., and Titley, S.R., 1981, Porphyry copper deposits. Part II. Hydrothermal alteration and mineralization: *ECONOMIC GEOLOGY* 75TH ANNIVERSARY VOLUME, p. 235–269.
- Berger, B.R., and Bethke, P.M., 1985, Geology and geochemistry of epithermal systems: *Society of Economic Geologists, Reviews in Economic Geology*, v. 2, 298 p.
- Bodnar, R.J., Cannatelli, C., de Vivo, B., Lima, A., Belkin, H.E., and Milia, A., 2007, Quantitative model for magma degassing and ground deformation (bradyseism) at Campi Flegrei, Italy: Implications for future eruptions: *Geology*, v. 35, p. 791–794.
- Bonafede, M., 1991, Hot fluid migration—an efficient source of ground deformation—application to the 1982–1985 crisis at Campi Flegrei-Italy: *Journal of Volcanology and Geothermal Research*, v. 48, p. 187–198.
- Boutwell, J.M., Keith, A., and Emmons, S.F., 1905, Economic geology of the Bingham mining district, Utah, with a section on areal geology, and an introduction on general geology: U.S. Geological Survey Professional Paper 38, 413 p.
- Bryant, B., 1988, Geology of the Farmington Canyon complex, Wasatch Mountains, Utah: U.S. Geological Survey Professional Paper 1476, 54 p.
- Bryant, B., and Nichols, D.J., 1988, Late Mesozoic and early Tertiary reactivation of an ancient crustal boundary along the Uinta trend and its interaction with the Sevier orogenic belt: *Geological Society of America Memoir 171*, p. 411–429.
- Burnham, C.W., 1979, Magmas and hydrothermal fluids, in Barnes, H.L., ed., *Geochemistry of hydrothermal ore deposits*, v. 2: New York, John Wiley and Sons, p. 71–136.
- Burnham, C.W., and Ohmoto, H., 1980, Late-stage processes of felsic magmatism: *Mining Geology Special Issue*, no. 8, p. 1–11.
- Cannell, J., Cooke, D.R., Walshe, J.L., and Stein, H., 2005, Geology, mineralization, alteration, and structural evolution of the El Teniente porphyry Cu-Mo deposit: *ECONOMIC GEOLOGY*, v. 100, p. 979–1003.
- Cappa, F., Rutqvist, J., and Yamamoto, K., 2009, Modeling crustal deformation and rupture processes related to upwelling of deep CO₂-rich fluids during the 1965–1967 Matsushiro earthquake swarm in Japan: *Journal of Geophysical Research-Solid Earth*, v. 114, article no. B10304.
- Carten, R.B., Geraghty, E.P., Walker, B.M., and Shannon, J.R., 1988, Cyclic development of igneous features and their relationship to high-temperature hydrothermal features in the Henderson porphyry molybdenum deposit, Colorado: *ECONOMIC GEOLOGY*, v. 83, p. 266–296.
- Cathles, L.M., and Shannon, R., 2007, How potassium silicate alteration suggests the formation of porphyry ore deposits begins with the nearly explosive but barren expulsion of large volumes of magmatic water: *Earth and Planetary Science Letters*, v. 262, p. 92–108.
- Constenius, K.N., 1996, Late Paleogene extensional collapse of the Cordilleran foreland fold and thrust belt: *Geological Society of America Bulletin*, v. 108, p. 20–39.
- Cook, S.J., and Bowman, J.R., 2000, Mineralogical evidence for fluid-rock interaction accompanying prograde contact metamorphism of siliceous dolomites: Alta stock aureole, Utah, USA: *Journal of Petrology*, v. 41, p. 739–757.
- Cox, S., in press, The application of failure mode diagrams for exploring the roles of fluid pressure and stress states in controlling styles of fracture-controlled permeability enhancement in faults and shear zones: *Geofluids*.
- Cox, S.F., Knackstedt, M.A., and Braun, J., 2001, Principles of structural control on permeability and fluid flow in hydrothermal systems: *Reviews in Economic Geology*, v. 14, p. 1–24.
- Cunningham, C.G., Austin, G.W., Naeser, C.W., Rye, R.O., Ballantyne, G.H., Stamm, R.G., and Barker, C.E., 2004, Formation of a paleothermal anomaly and disseminated gold deposits associated with the Bingham Canyon porphyry Cu-Au-Mo system, Utah: *ECONOMIC GEOLOGY*, v. 99, p. 789–806.
- Deino, A., and Keith, J.D., 1998, Ages of volcanic and intrusive rocks in the Bingham mining district, Utah: *Society of Economic Geologists Guidebook Series*, v. 29, p. 91–100.
- Delaney, P.T., Pollard, D.D., Ziony, J.I., and McKee, E.H., 1986, Field relations between dikes and joints—emplacement processes and paleostress analysis: *Journal of Geophysical Research-Solid Earth and Planets*, v. 91, p. 4920–4938.
- Dilles, H.J., 1987, Petrology of the Yerington batholith, Nevada: Evidence for evolution of porphyry copper ore fluids: *ECONOMIC GEOLOGY*, v. 82, p. 1750–1789.
- Dzurisin, D., Lisowski, M., and Wicks, C.W., 2009, Continuing inflation at Three Sisters volcanic center, central Oregon Cascade Range, USA, from GPS, leveling, and InSAR observations: *Bulletin of Volcanology*, v. 71, p. 1091–1110.
- Einaudi, M.T., 1992, Ore deposits in the Oquirrh and Wasatch Mountains, Utah—examples of large-scale water-rock interaction: *Water-Rock Interaction*, v. 1 and 2, p. 879–883.
- , 1997, Mapping altered and mineralized rocks: An introduction to the Anaconda method: Stanford, CA, Stanford University.
- , 2000, Skarns of the Yerington district, Nevada: A trip log and commentary: *Society of Economic Geologists Guidebook Series*, v. 32, p. 101–126.
- English, J.M., and Johnston, S.T., 2004, The Laramide orogeny: What were the driving forces?: *International Geology Review*, v. 46, p. 833–838.

- Fournier, R.O., 1983, A method of calculating quartz solubilities in aqueous sodium-chloride solutions: *Geochimica et Cosmochimica Acta*, v. 47, p. 579–586.
- , 1999, Hydrothermal processes related to movement of fluid from plastic into brittle rock in the magmatic-epithermal environment: *ECONOMIC GEOLOGY*, v. 94, p. 1193–1211.
- Gruen, G., 2007, Distribution and orientation of veins in the Bingham Canyon porphyry Cu-Mo-Au deposit, Utah: Unpublished M.Sc. thesis, Switzerland, ETH Zurich, 123 p.
- Gustafson, L.B., and Hunt, J.P., 1975, The porphyry copper deposit at El-Salvador, Chile: *ECONOMIC GEOLOGY*, v. 70, p. 857–912.
- Heidrick, T.L., and Titley, S.R., 1982, Fracture and dike patterns in Laramide plutons and their structural and tectonic implications: American southwest, in Titley, S.R., ed. *Advances in geology of the porphyry copper deposits, southwestern North America*: Tucson, AZ, University of Arizona Press, p. 73–91.
- Hurwitz, S., Christiansen, L.B., and Hsieh, P.A., 2007, Hydrothermal fluid flow and deformation in large calderas: Inferences from numerical simulations: *Journal of Geophysical Research-Solid Earth*, v. 112, article no. B02206.
- Hutnak, M., Hurwitz, S., Ingebritsen, S.E., and Hsieh, P.A., 2009, Numerical models of caldera deformation: Effects of multiphase and multicomponent hydrothermal fluid flow: *Journal of Geophysical Research-Solid Earth*, v. 114, article no. B04411.
- Jagoutz, O., Muntener, O., Ulmer, P., Pettke, T., Burg, J.P., Dawood, H., and Hussain, S., 2007, Petrology and mineral chemistry of lower crustal intrusions: the Chilas Complex, Kohistan (NW Pakistan): *Journal of Petrology*, v. 48, p. 1895–1953.
- John, D.A., 1989, Geologic setting, depths of emplacement, and regional distribution of fluid inclusions in intrusions of the Central Wasatch Mountains, Utah: *ECONOMIC GEOLOGY*, v. 84, p. 386–409.
- , 1998, Geologic setting and characteristics of mineral deposits in the central Wasatch Mountains, Utah: Society of Economic Geologists Guidebook Series, v. 29, p. 11–33.
- John, E.C., 1978, Mineral zones in the Utah copper orebody: *ECONOMIC GEOLOGY*, v. 73, p. 1250–1259.
- Jolly, R.J.H., and Sanderson, D.J., 1997, A Mohr circle construction for the opening of a pre-existing fracture: *Journal of Structural Geology*, v. 19, p. 887–892.
- Karlstrom, K.E., Whitmeyer, S.J., Dueker, K., Williams, M.L., Levander, A., Humphreys, G., Keller, G.R., and Group, C.-R.W., 2005, 4-D image of the lithosphere beneath the Rocky Mountains and implications for understanding the evolution of continental lithosphere: *Geophysical Monograph*, v. 154, 482 p.
- Kelly, W.C., and Rye, R.O., 1979, Geologic, fluid inclusion, and stable isotope studies of the tin-tungsten deposits of Panasqueira, Portugal: *ECONOMIC GEOLOGY*, v. 74, p. 1721–1822.
- Klemm, L.M., Pettke, T., Heinrich, C.A., and Campos, E., 2007, Hydrothermal evolution of the El Teniente deposit, Chile: Porphyry Cu-Mo ore deposition from low-salinity magmatic fluids: *ECONOMIC GEOLOGY*, v. 102, p. 1021–1045.
- Landtwing, M.R., 2004, Fluid evolution and ore mineral precipitation at the Bingham porphyry Cu-Au-Mo deposit, Utah, deduced from cathodoluminescence imaging and LA-ICPMS microanalysis of fluid inclusions: Unpublished Ph.D. thesis, Switzerland, ETH Zurich, 260 p.
- Landtwing, M.R., Pettke, T., Halter, W.E., Heinrich, C.A., Redmond, P.B., Einaudi, M.T., and Kunze, K., 2005, Copper deposition during quartz dissolution by cooling magmatic-hydrothermal fluids: The Bingham porphyry: *Earth and Planetary Science Letters*, v. 235, p. 229–243.
- Landtwing, M.R., Furrer, C., Pettke, T., Guillong, M., and Heinrich, C.A., 2010, The Bingham Canyon porphyry Cu-Mo-Au deposit: III. Zoned copper-gold ore deposition by magmatic vapor expansion: *ECONOMIC GEOLOGY*, v. 105, p. 91–118.
- Lanier, G., John, E.C., Swensen, A.J., Reid, J., Bard, C.E., Caddey, S.W., and Wilson, J.C., 1978, General geology of the Bingham mine, Bingham Canyon, Utah: *ECONOMIC GEOLOGY*, v. 73, p. 1228–1241.
- Lima, A., de Vivo, B., Spera, F.J., Bodnar, R.J., Milia, A., Concettina, N., Belkin, H.E., and Cannatelli, C., 2009, Thermodynamic model for uplift and deflation episodes (bradyseism) associated with magmatic-hydrothermal activity at the Campi Flegrei (Italy): *Earth-Science Reviews*, v. 97, p. 44–58.
- Mardia, K.V., 1975, Statistics of directional data: *Journal of the Royal Statistical Society, Series B: Methodological*, v. 37, p. 349–393.
- Maughan, D.T., Keith, J.D., Christiansen, E.H., Pulsipher, T., Hattori, K., and Evans, N.J., 2002, Contributions from mafic alkaline magmas to the Bingham porphyry Cu-Au-Mo deposit, Utah, USA: *Mineralium Deposita*, v. 37, p. 14–37.
- Melker, M.D., and Geissman, J.W., 1998, Paleomagnetism of the Oquirrh Mountains and implications for the Cenozoic structural history of the easternmost Great Basin: *Society of Economic Geologists Guidebook Series*, v. 29, p. 101–112.
- Nakamura, K., 1977, Volcanos as possible indicators of tectonic stress orientation—principle and proposal: *Journal of Volcanology and Geothermal Research*, v. 2, p. 1–16.
- Parry, W.T., Wilson, P.N., and Bruhn, R.L., 1988, Pore-fluid chemistry and chemical-reactions on the Wasatch normal-fault, Utah: *Geochimica et Cosmochimica Acta*, v. 52, p. 2053–2063.
- Parry, W.T., Jasumback, M., and Wilson, P.N., 2002, Clay mineralogy of phyllic and intermediate argillic alteration at Bingham, Utah: *ECONOMIC GEOLOGY*, v. 97, p. 221–239.
- Phillips, C.H., Smith, T.W., and Harrison, E.D., 1998, Alteration, metal zoning, and ore controls in the Bingham Canyon porphyry copper deposits, Utah: *Society of Economic Geologists Guidebook Series*, v. 29, p. 133–145.
- Presnell, R.D., 1992, Geology and geochemistry of the Barneys Canyon gold deposit, Salt Lake County, Utah: Unpublished Ph.D. thesis, Salt Lake City, UT, University of Utah, 363 p.
- , 1998, Structural controls on the plutonism and metallogeny in the Wasatch and Oquirrh Mountains, Utah: *Society of Economic Geologists Guidebook Series*, v. 29, p. 1–9.
- Presnell, R.D., and Parry, W.T., 1995, Evidence of Jurassic tectonism in the Oquirrh Mountains from the Barneys Canyon gold deposit: *Geological Society of America Special Paper* 299, p. 313–326.
- Redmond, P.B., 2002, Magmatic-hydrothermal fluids and copper-gold ore formation at Bingham Canyon, Utah: Unpublished Ph.D. thesis, Stanford, CA, Stanford University, 228 p.
- Redmond, P.B., and Einaudi, M.T., 2010, The Bingham Canyon porphyry Cu-Mo-Au deposit: I. Sequence of intrusion, vein formation, and sulfide deposition: *ECONOMIC GEOLOGY*, v. 105, p. 43–68.
- Redmond, P.B., Landtwing, M.R., and Einaudi, M.T., 2001, Cycles of porphyry dike emplacement, veining, alteration and mineralization in the Bingham porphyry Cu-Au-Mo deposit, Utah: *Mineral Deposits at the Beginning of the 21st Century, Joint Biennial SGA-SEG Meeting*, 6th, Krakow, Poland, August, 2001, Proceedings, p. 473–476.
- Redmond, P.B., Einaudi, M.T., and Landtwing, M.R., 2002, Cyclical P-T-X evolution of magmatic-hydrothermal fluids in the Bingham porphyry Cu-Au-Mo deposit, Utah: *Geological Society of America paper* 82-12.
- Redmond, P.B., Einaudi, M.T., Inan, E.E., Landtwing, M.R., and Heinrich, C.A., 2004, Copper deposition by fluid cooling in intrusion-centered systems: New insights from the Bingham porphyry ore deposit, Utah: *Geology*, v. 32, p. 217–220.
- Richards, J.P., 2003, Tectono-magmatic precursors for porphyry Cu-(Mo-Au) deposit formation: *ECONOMIC GEOLOGY*, v. 98, p. 1515–1533.
- Robin, P.Y.F., and Jowett, E.C., 1986, Computerized density contouring and statistical evaluation of orientation data using counting circles and continuous weighting functions: *Tectonophysics*, v. 121, p. 207–223.
- Rohrlach, B.D., and Loucks, R.R., 2005, Multi-million-year cyclic ramp-up of volatiles in a lower crustal magma reservoir trapped below the Tampakan copper-gold deposit by Mio-Pliocene crustal compression in the southern Philippines, in Porter, T.M., ed., *Super porphyry copper and gold deposits: A global perspective*, v. 2: Adelaide, PGC Publishing, 43 p.
- Rohrlach, B.D., Loucks, R.R., and Palin, J.M., 2003, Isochoric ascent of lithostatically-pressure, dense magmatic vapor during gold-enargite ore formation: *Geochimica et Cosmochimica Acta*, v. 67, p. A401.
- Rose, A.W., 1970, Zonal relations of wallrock alteration and sulfide distribution at porphyry copper deposits: *ECONOMIC GEOLOGY*, v. 65, p. 920–936.
- Rusk, B.G., and Reed, M.H., 2002, Scanning electron microscope-cathodoluminescence analysis of quartz reveals complex growth histories in veins from the Butte porphyry copper deposit, Montana: *Geology*, v. 30, p. 727–730.
- Sawkins, F.J., 1990, Metal deposits in relation to plate tectonics: Berlin, Springer-Verlag, 461 p.
- Sears, J.W., Graff, P.J., and Holden, G.S., 1982, Tectonic evolution of Lower Proterozoic rocks, Uinta Mountains, Utah and Colorado: *Geological Society of America Bulletin*, v. 93, p. 990–997.
- Seedorff, E., Dilles, J.H., Proffett, J.M., Jr., Einaudi, M.T., Zurcher, L., Stavast, W.J.A., Johnson, D.A., and Barton, M.D., 2005, Porphyry deposits: Characteristics and origin of hypogene features: *ECONOMIC GEOLOGY* 100th ANNIVERSARY VOLUME, p. 251–298.

- Sillitoe, R.H., 1972, Relation of metal provinces in Western America to subduction of oceanic lithosphere: Geological Society of America Bulletin, v. 83, p. 813–817.
- Sillitoe, R.H., 2010, Porphyry copper systems: *ECONOMIC GEOLOGY*, v. 105, p. 3–41.
- Sillitoe, R.H., and Perello, J., 2005, Andean copper province: Tectonomagnetic settings, deposit types, metallogeny, exploration, and discovery: *ECONOMIC GEOLOGY 100TH ANNIVERSARY VOLUME*, p. 845–890.
- Simmons, S.F., White, N.C., and John, D.A., 2005, Geological characteristics of epithermal precious and base metal deposits: *ECONOMIC GEOLOGY 100TH ANNIVERSARY VOLUME*, p. 485–522.
- Skewes, M.A., Arévalo, A., Floody, R., Zuñiga, P. H., and Stern, C.R., 2002, The giant El Teniente breccia deposit: Hypogene copper distribution and emplacement: Society of Economic Geologists Special Publication 9, p. 299–332.
- Smith, W.H., 1961, The volcanics of the eastern slopes of the Bingham District, Utah: Utah Geological Society Guidebook, p. 101–119.
- Stephens, J.R., Mair, J.L., Oliver, N.H.S., Hart, C.J.R., and Baker, T., 2004, Structural and mechanical controls on intrusion-related deposits of the Tombstone gold belt, Yukon, Canada, with comparisons to other vein-hosted ore-deposit types: *Journal of Structural Geology*, v. 26, p. 1025–1041.
- Swensen, A.J., 1975, Sedimentary and igneous rock of the Bingham district, in Bray, R.E., and Wilson, J.C., eds., *Guide Book to the Bingham mining district: Bingham Canyon, UT, United States*, Society of Economic Geologists, Kennebott Copper Corp., p. 21–39.
- Titley, S.R., 1982, *Advances in Geology of the Porphyry Copper Deposits, Southwestern North America*: Tucson, AZ, United States, University of Arizona Press, 560 p.
- Titley, S.R., 2001, Crustal affinities of metallogenesis in the American Southwest: *ECONOMIC GEOLOGY*, v. 96, p. 1323–1342.
- Todesco, M., Rutqvist, J., Chiodini, G., Pruess, K., and Oldenburg, C.I.M., 2004, Modeling of recent volcanic episodes at Phlegrean Fields (Italy): Geochemical variations and ground deformation: *Geothermics*, v. 33, p. 531–547.
- Tooker, E.W., Roberts, R.J., Gordon, M.J., and Duncan, H.M., 1970, Upper Paleozoic rocks in the Oquirrh Mountains and Bingham mining district, Utah, with a section on biostratigraphy and correlation, U.S. Geological Survey Professional Paper 629–A, p. A1–A76.
- Tosdal, R.M., and Richards, J.P., 2001, Magmatic and structural controls on the development of porphyry Cu ± Mo ± Au deposits: *Reviews in Economic Geology*, v. 14, p. 157–181.
- Townend, J., and Zoback, M.D., 2000, How faulting keeps the crust strong: *Geology*, v. 28, p. 399–402.
- Ulrich, T., Günther, D., and Heinrich, C.A., 2001, The evolution of a porphyry Cu-Au deposit, based on LA-ICP-MS analysis of fluid inclusions: Bajo de la Alumbra, Argentina: *ECONOMIC GEOLOGY*, v. 96, p. 1743–1774.
- Waite, K.A., Keith, J.D., Christiansen, E.H., Whitney, J.A., Hattori, K., Tingey, D.G., and Hook, C.J., 1998, Petrogenesis of the volcanic and intrusive rocks associated with the Bingham Canyon porphyry Cu-Au-Mo deposit, Utah: *Society of Economic Geologists Guidebook Series*, v. 29, p. 69–90.
- Warnaars, F.W., Smith, W.H., Bray, R.E., Lanier, G., and Shafiqullah, M., 1978, Geochronology of igneous intrusions and porphyry copper mineralization at Bingham, Utah: *ECONOMIC GEOLOGY*, v. 73, p. 1242–1249.
- Williams-Jones, A.E., and Heinrich, C.A., 2005, Vapor transport of metals and the formation of magmatic-hydrothermal ore deposits: *ECONOMIC GEOLOGY*, v. 100, p. 1287–1312.
- Zoback, M.L., 1983, Structure and Cenozoic tectonism along the Wasatch fault zone, Utah: *Geological Society of America Memoirs* 157, p. 3–27.

APPENDIX

Graphical Representation and Statistical Analysis

Orientation data for each vein type at each of the bench mapping locations were entered in a database for statistical analysis and stereographic plotting of directional data, using SpheriStat 2.2 for Windows (Pangaea Scientific, 1990–1998). Some closely adjacent mapping locations in the same lithology were combined to obtain a statistically meaningful and more even spatial distribution of 26 mapping areas (Fig. 6).

Vein orientations were recorded as dip and dip direction of the veins and plotted as poles perpendicular to the vein plane in stereograms, projected to the lower hemisphere by equal-area projection (Mardia, 1975; Figs. 6, 8). The dominantly steep quartz-pyrite veins were also displayed in rose diagrams to show the relative frequency of strike directions, irrespective of the vein dips (Fig. 7).

Contouring of three-dimensional orientation data was carried out with SpheriStat, using the Gaussian smoothing method (Robin and Jowett, 1986). The point density is estimated by counting the number of data records with a certain angular distance from the counting station, the particular direction at which the point density is being estimated (Pangaea Scientific, 1990–1998). How much each measurement contributes to the total count depends upon a weighting function. Gaussian smoothing includes all measurements but weighs their contribution to the count by the Fisher function:

$$w = \exp[k(\cos(t)-1)], \quad (A1)$$

where t is the angular distance from the counting station and k is the kurtosis. This bell-shaped function is smooth and

diminishes rapidly with angular distance. The choice of the k value affects the resolving power of the counting and determines which variation of the Gaussian method is applied. Contouring with a higher kurtosis yields a contour surface with sharper peaks and valleys, i.e., having a higher “frequency content.” In this study, a k value of 100 has been chosen. The expected count E is given by:

$$E = N/k, \quad (A2)$$

where N is the total number of data records. The standard deviation S is the square root of the variance V , which represents the integral of $(w-E)(w-E)$ over the half-sphere. The fractional area is $1/k$, in this case 1 percent of the hemisphere. Five contour levels have been chosen: 2, 4, 6, 8, and 10 (Fig. 8), which are dimensionless values in multiples of the standard deviation above the expected count.

Principal directions of all directional measurements were also calculated in SpheriStat 2.2. Unlike the point density distribution, which measures the local clustering of directions, the principal directions measure the average clustering for the dataset as a whole. SpheriStat (Pangaea Scientific, 1990–1998) calculates the principal directions as a set of three orthogonal, so-called principal vectors, where [1] represents the least and [3] is the highest accumulation of data points. Accordingly, [2] is the intermediate accumulation of points; therefore [1] < [2] < [3] (see Fig. 8).